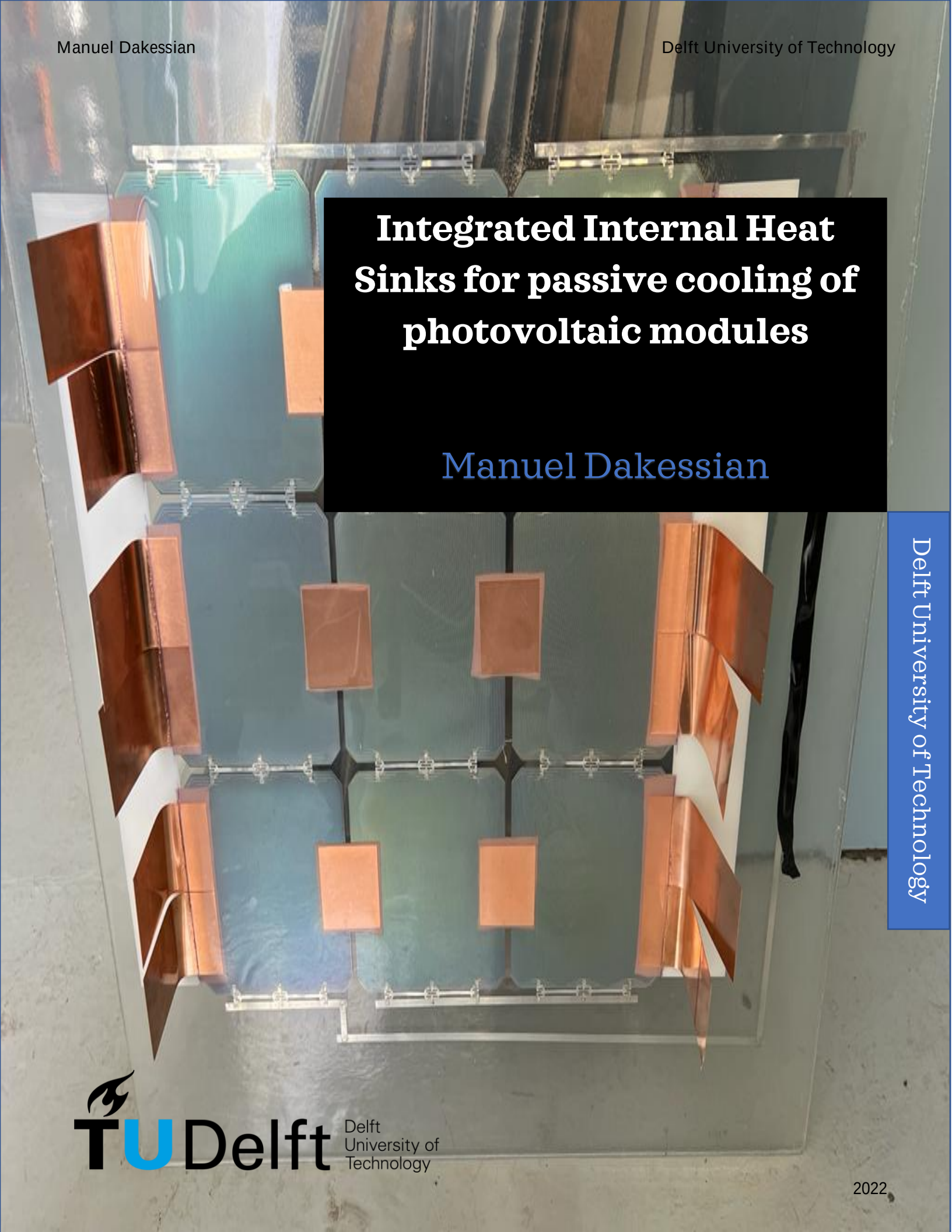

Integrated Internal Heat Sinks for passive cooling of photovoltaic modules

Manuel Dakessian

Delft University of Technology

TU Delft Delft University of Technology

2022

Delft University of Technology

Master Thesis

Integrated Internal Heat Sinks for passive cooling of photovoltaic modules

Author:
Manuel Dakessian
5202531

Supervisors:
Dr. ir. Hesan Ziar
ir. Juan Camilo Ortiz Lizcano

A thesis submitted in partial fulfillment of the requirements for the degree of MSc Sustainable Energy Technology

in the

Photovoltaic Material and Devices Group TU Delft

To be defended publicly on Friday July 15, 2022 at 10:00 AM

Thesis committee:

Dr. ir. Hesan Ziar

Prof. Dr. Kamel Hooman

Dr. ir. Rudi Santbergen

ir. Juan Camilo Ortiz Lizcano

Ճանաչել զիմաստութիւն եւ զխրատ
Իմանալ զբանս հանճարոյ

-Մեսրոպ Մաշտոց, 405

To recognize wisdom and guidance
To know the creations of the greats

-Mesrop Mashtots, 405

Acknowledgements

This thesis is the result of a combination of experimental and theoretical work for over a period of seven months at the Photovoltaic Materials and Devices group of TU Delft. None of this would be possible without the guidance of everyone involved in the group.

First of all, I would like to thank Dr. Hesan Ziar for giving me the chance to work on this project. I always thought that finding a project which would fit perfectly with my background and interests would be an impossible task. I can honestly say that the period of my life spent on this project has been one of the most fun and insightful experiences of my life. I would also like to thank you professor for your constructive criticism, patience and most importantly freedom in my line of thought throughout the entire project.

Special thanks to Juan Camilo for guiding me through every step of the project. You were always there to answer any question I had and provide the support I needed to focus on myself and the project. Thank you for sharing your own experience and knowledge, not only from an academic perspective. I wish you nothing but the best for your PhD research, may you always inspire students as you inspired me and share your optimism.

I would like to thank all the researchers who helped me untangle every obstacle I faced throughout the project and all the technicians who patiently helped order and deliver all the material I needed.

I am also thankful for Prof. Dr. Kamel Hooman and Dr. ir. Rudi Santbergen for being part of my thesis committee.

On a more personal note, I would like to thank all the people who I've met throughout my masters at Delft, you have made me understand the true meaning of work hard, play harder. You have made these two years unforgettable.

Most importantly, I would like to thank my family who have always been there for me. You have given me strength when I've felt weak, guidance when I've felt lost and support well always. I cannot express how grateful I am.

Contents

List of Figures

List of Tables

List of Abbreviations

A	Cross sectional area perpendicular to heat flow
C	Center
E	Edge
EL	Electroluminescence
EVA	Ethylene Vinyl Acetate
FBC	Front/Back Contacted
IBC	Integrated Back Contact
Isc	Short Circuit Current
K	Thermal Conductivity
LASS	Large Area Solar Simulator
ME	Metal Edge
PCM	Phase Change Material
Pmax	Maximum power
PV	Photovoltaics
R	Thermal Resistivity
Voc	Open Circuit Voltage
Δx	Thickness parallel to heat flow

Abstract

High operating temperatures harm photovoltaic (PV) modules. The increase in temperature of the cells leads to lower open circuit voltage and higher short circuit current ultimately leading to a lower power output due to a negative thermal coefficient. Hence, lowering the temperature of commercial crystalline silicon modules during their operation becomes desirable, as it increases the system's energy yield and prolongs the module's lifespan. Throughout the years several attempts have been made to decrease the temperature of PV modules, characterized my two main groups of cooling techniques, active and passive cooling techniques. Active cooling techniques require additional power to cool the panels whereas passive cooling techniques rely on natural convection and require no additional power input.

In this thesis, we experimentally investigate the cooling potential of a novel passive cooling method that integrates an internal heat sink into PV modules. The basic idea of the technology is to create a thermal circuit beneath the solar cell that allows for the extraction of the heat directly from the solar cell to the outside environment. The experiments started on a single solar cell, to find the best configuration. We adapted the optimized design onto a 2x2 PV and a 3x3 PV module. Finally, the internal heat sinks were connected to a frame. We observed a temperature reduction of around 4-5°C on the module with the internal heat sink compared to a Standard module under the same environmental conditions.

Introduction

Solar energy is the most abundant form of renewable energy in the world. With the increase in emissions from fossil fuel combustion, PV system installations have increased worldwide to produce electricity. The performance of PV panels strongly depends on different environmental factors such as solar irradiance, ambient temperature, wind speed, and wind direction (J.G. Hernandez-Perez, 2021). This master thesis project aims at reducing the effect that solar irradiance and ambient temperature have on the efficiency and lifetime of PV panels. By introducing an internal heat sink in direct contact with the backside of the cells, we aim to bypass the EVA and Tedlar layer, which have low thermal conductivity and pass the heat directly through the heat sink to the outside environment.

1 Literature Review

The temperature of a PV panel increases with solar irradiance since only a fraction of the energy absorbed produces electricity. It is also affected by the surrounding ambient temperature. Temperature is a significant factor that negatively affects the operation of a PV system. Studies show that, in the case of crystalline silicon modules (c-Si), solar cell temperatures above 25 °C can decrease in efficiency from 0.25%/◦C up to 0.5%/◦C (Escobar et al., 2021). The operating temperature of a PV panel is around 50-60 ◦C. High temperatures reduce open-circuit voltage and fill factor and increase the recombination of internal charge carriers, which lowers output power. Moreover, thermal cycles accelerate the aging of the PV panels and lead to degradation of performance (novergy, 2020).

Two cooling methods exist to cool PV panels: active and passive. Active cooling techniques require additional power supply due to the use of fans and pumps to force fluid flow over the PV panel and reduce operating temperature. The disadvantage of this method is the need for additional power, which reduces overall efficiency. Passive cooling requires no additional power; several studies have been done on different passive cooling techniques. Passive cooling techniques include floating systems on water, using phase change material, and installing heat sinks on the panels. The temperature of the PV module ranges from 32.8 to 90.0 ◦C, depending on the working and environmental conditions (A.M. Elbreki, 2021). Different passive and active cooling techniques have resulted in a lower PV module temperature range from 25.0 to 65.7 ◦C and 32–70 ◦C for passive and active cooling approaches, respectively (A.M. Elbreki, 2021).

Summary of research done on reducing cell temperature with passive cooling techniques:

Table 1- Passive cooling techniques for PV modules

Heatsink design	Reference	Temperature reduction achieved	Efficiency
A finned aluminum plate attached with thermal grease	(Ahmad El Mays, 2017)	6.1 °C on PV panel surface	Increase in electrical conversion by 1.75%
Aluminum perforated ribs	(CG Popovici, 2016)	Average of 10 °C on PV cell	Increase of 7.55% in power output
Discontinuous finned heatsink	(J.G. Hernandez-Perez, 2021)	Average of 6 °C on PV cell	Increase of 3.66% in power output
Internally finned phase change material heat sink	(M.J. Huang, 2011)	Average of 8 °C	Increase of 4.27% in power output
Passive cooling with lapping fins	(A.M. Elbreki, 2021)	Average of 24°C	Overall efficiency increases by 10.68%
Different fins attached with thermal paste	(Bayrak, Oztop, & Selimefendigil, 2019)	3.39 °C on PV panel back surface	An increase of 9.4W in power output
Thermal glue used to attach Aluminum ribs	(Grubišić-Čabo, Papadopoulos, Kragić, Čoko, & Nižetic, 2017)	Average of 8°C	Increase of 5% in electrical conversion
Aluminum fins with pores	(Selimefendigil, Bayrak, & Oztop, 2018)	Average of 0.36°C on PV back surface	An increase of 7.26W in power output
Aluminum Heat Spreaders and cotton wick	(Chandrasekar & Senthilkumar, 2015)	5.9 °C on PV panel back surface	Increase of 14% in electrical generation
Aluminum perforated ribs	(Popovici, Hudişteanu, Mateescu, & Cherecheş, 2016)	Average of 10°C	Increase of 7.55% in power output
Phase change material in a finned container heat sink	(Wongwuttanasatian, Sarikarin, & Suksri, 2020)	Average of 6.1°C	Increase of 5.3% in power output
Yellow petroleum jelly as phase change material	(Indartono, Suwono, & Pratama, 2014)	Maximum of around 4.4°C	Increase of an average of 6.5% in power output
Natural water flow cooling the backside of a PV panel	(Sharaf, Yousef, & Huzayyin, 2011)	Around 30°C	Increase of 12% in conversion efficiency

Summary of research done on reducing cell temperature with active cooling techniques:

Table 2- Active cooling techniques for PV modules

Cooling design	Reference	Temperature reduction achieved	Efficiency
Water Spraying on the front surface of the PV panel	(S. Nizetic, 2016)	Max of 20◦C	Increase of 14.6% in power output
Liquid immersion cooling in water at a depth of 1 cm	(S. Mehrotra S, 2014)	Around 40◦C	Increase of 17.8% in power output
Forced air stream on a PV panel	(R. Mazon-Hernandez, 10)	Max of 15◦C	Overall efficiency increases by 2%
Water flow over the front of PV panels	(Krauter, 2004)	Around 22◦C	Increase of 10.3% in power output
Solar cells immersed in dielectric liquids	(Xinyue Han, 2011)	Around 30◦C	NA
PV/T thermal cooling system	(Teo, Lee, & Hawlader, 2012)	Around 30◦C	Increase of 18.5% in power output

Studies have created different concepts with a wide range of temperature reductions, where in most cases, the temperature reduction achieved by active cooling methods is higher.

This report focuses solely on creating a passive cooling technique to help reduce the temperature of the PV module; hence more research has gone into the literature regarding passive cooling techniques. A summary of some of this research is available in the following section:

Passive PV module cooling under free convection through Vortex Generation

In this paper, the researchers attach vortex generators arranged in an array to the back side of a PV module. The vortex generators' cooling ability was assessed using infrared thermography, and different spacings for the vortex generators were tested. The research concluded that vortex generators made up of thermally non-conductive material could reduce the temperature of a PV module by 2°C. In contrast, vortex generators made of thermally conductive material could reduce the temperature of the PV module up to around 3°C. The decrease in temperature of the PV module was induced by mixing in the boundary layer, enhancing convection on the rear of the PV module. The vortices generated depend strongly on the vortex generator's dimensions, aerodynamic structure, and placement. The best-case scenario for a rectangular wing vortex generator is a horizontal spacing of around

3cm for thermally non-conductive material and 2cm for thermally conductive material. (Zhou et al., 2022)

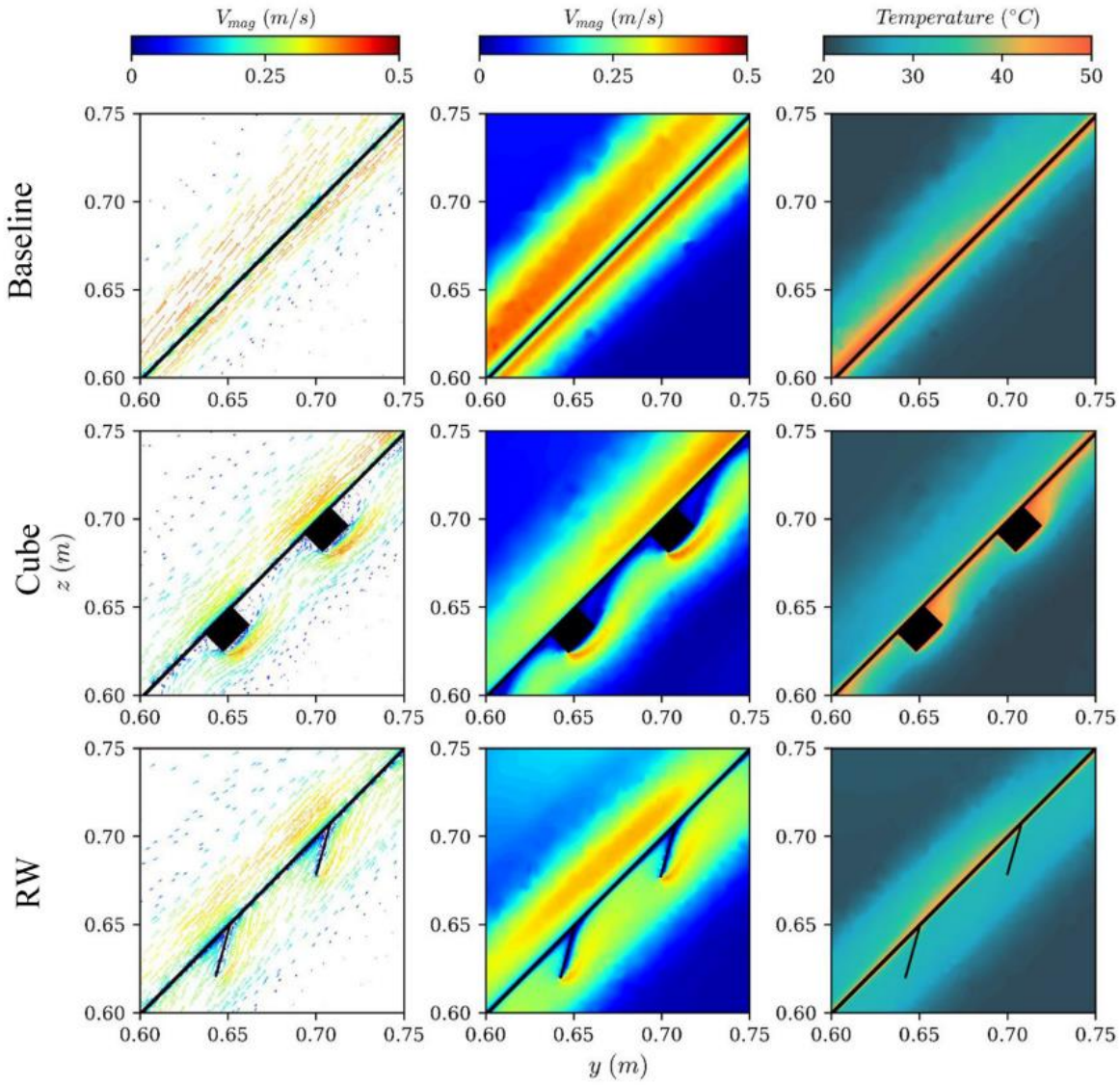

Figure 1- A comparison of simulated velocity vectors (left), color contours of velocity (center), and temperature (right) on a spanwise cross-section (YZ plane). The cases for baseline (top), PLA cube VGs (middle), and PLA RW VGs (bottom) (Zhou et al., 2022)

Passive PV module cooling with the use of aluminum heat sinks

This research paper used an aluminum heat sink to dissipate heat from the PV cell. Experiments used a solar simulator and considered different ambient temperatures and illumination intensities. A maximum increase of 20 % in power output was observed under irradiance values of around 800W/m2. Maximum cooling, around 30%, occurred under irradiance of around 600W/m2. (Cuce, Bali, & Sekucoglu, 2011)

Improving the Electrical Parameters of a Photovoltaic Panel employing an Induced Air Stream

In this research paper, an airflow channel has been added to the backside of the PV panel to induce an air stream. Observations showed that the depth of the flow channel has a significant impact on the passive cooling capabilities. For a PV module length-to-channel depth ratio of around 0.085, the PV module is heated up by around 5-6°C with regards to a PV module of the regular mount. The research concluded that a passive flow channel beneath the PV module has a reverse impact on the PV module cooling, hence should be avoided. (Mazón-Hernández, García-Cascales, Vera-García, Káiser, & Zamora, 2013).

Figure 2-Natural convection configuration of passive air stream (Mazón-Hernández, García-Cascales, Vera-García, Káiser, & Zamora, 2013)

Experimental and economic analysis of passive cooling PV module using fins and planar reflector

In this research paper, researchers tested the performance of a PV panel with two finned heat sink designs, lapping and longitudinal. Experiments aimed at identifying the optimum design parameters of the fins in height, pitch, thickness, number, and tilt angle. The experiment, done under actual environmental conditions, had an average irradiance of 1000W/m2 and an ambient temperature of 33°C. The experiments concluded that passive cooling using looping fins had the best performance, observing a temperature reduction of 24.6°C compared to the standard PV module. This reduction implied an improvement of around 10.68% in electrical efficiency. A Life Cycle Cost Analysis was also conducted, which showed that longitudinal fins had a payback period of around 4.2 years, whereas lapping fins had a payback period of 5 years, compared to the standard PV module, which has a payback period of 8.4 years. The study concludes that the optimum length of both

longitudinal and lapping fins is 200mm, and the optimum number of fins for lapping and longitudinal fins heat sink are 18 and 15, respectively. (A.M. Elbreki, 2021)

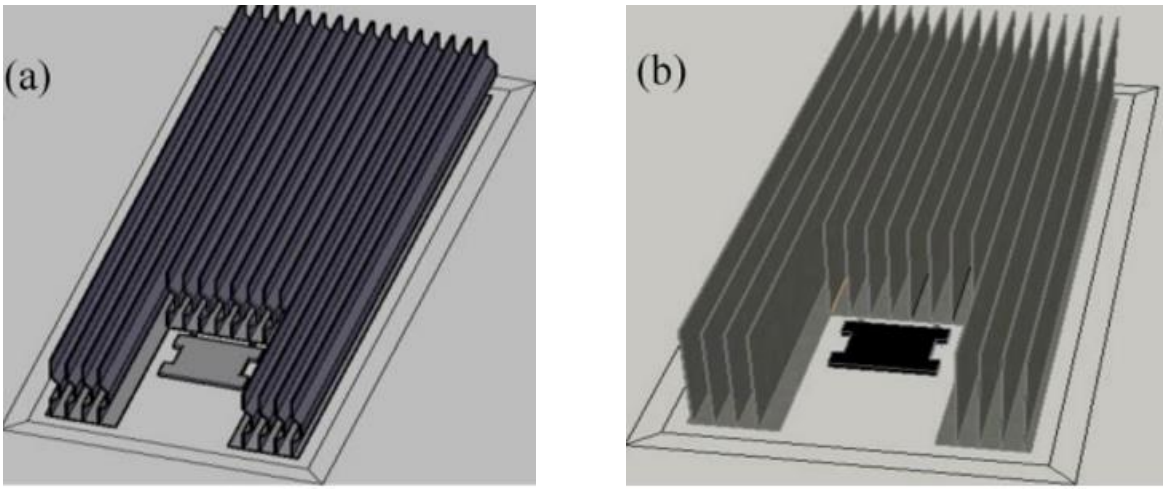

Figure 3- Schematic of a) PV module with Lapping Fins b) PV module longitudinal fins (A.M. Elbreki, 2021)

Infrared optical filters for passive cooling of photovoltaic modules

This research paper has created a thermal model in COSMOL to study the effect of adding optical filters to block undesired irradiation in the infrared region. In the infrared region, the photons have longer wavelengths, hence less energy. These photos do not have enough energy to overcome the bandgap of the PV cell; hence their energy is converted into heat via free-carrier absorption effects. The study determined the progressive increase of module temperature due to the absorption of different wavelengths of light. It showed that a total reflectance of light between wavelengths 1100-2500nm would decrease PV module temperature by around 5 to 6°C. A multilayer structure based on 90 to 100 layers would be able to reflect around 90% of the incident IR light. A more straightforward structure based on 44 layers could be used instead for simplicity. This filter can reflect most wavelengths between 1100 and 2000nm, a good alternative for the significant reduction in layers needed. However, subsequent depositions revealed significant complications during the fabrication of the structure, and research on its development is still underway. (Silva, 2017)

Discontinuous finned heat sink profile for passive cooling of photovoltaic modules

This research paper studies a segmented fin heatsink to see its effect on reducing PV module temperature. Compared to a conventional continuous heatsink, the segmented fin heatsink outperforms its heat extraction capacity. Researchers created a computational model to study the effect of the width of fins on hydraulic performance and temperature

level. The computational model showed a temperature reduction potential of around 7°C. A 20mm wide fin was found to be the optimal fin width, and compared to the numerical model, it performed well in the outdoor experiment, reducing the temperature of the PV module by around 5°C. The proposed heatsink also showed lower pressure losses than the conventional heat sink geometry by decreasing the flow velocity losses in the channel, promoting convective heat flow (J.G. Hernandez-Perez, 2021).

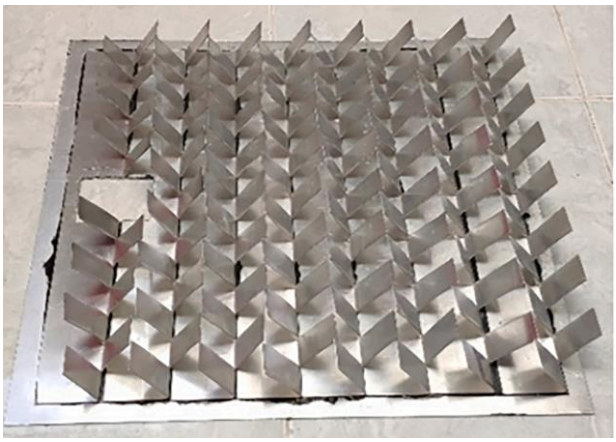

Figure 4- Segmented heat sink design (J.G. Hernandez-Perez, 2021)

Passive cooling of PV modules by using phase change material in a finned container heat sink

In this research paper, palm wax, a phase change material, was used to reduce the temperature of the solar module. The grooved, tubed, and finned containers were the three different phase change material containers. Finned containers provided the most cooling. The increase in the cooling effect from the PCM material leads to an increase in electrical power output. Compared to a standard PV module, it was found that the finned container was able to reduce the module's temperature by 6.1°C, from 57.9°C to 51.8°C, and the efficiency of the PV module improved by around 5.3%. The study also concluded that the PCM material was unnecessary in cooling when the solar irradiance was lower than 500W/m2. However, it enhanced cooling for all levels of irradiance higher than 500W/m2 (Wongwuttanasatian, Sarikarin, & Suksri, 2020).

(a) (b) (c)

Figure 5- Heat Sinks with PCM a) Grooved b) Tubed c) Finned (Wongwuttanasatian, Sarikarin, & Suksri, 2020)

2 Methodology

All the concepts mentioned in the literature review section try to remove the heat from the outer layer of the PV panels by attaching thermally conductive material to the PV panel or forcing flow over and under it. This research focuses on extracting heat from the IBC solar cell toward the outside environment.

IBC solar cells are selected mainly for their robustness compared to FBC. Moreover, they are less prone to manufacturing cracks during interconnection. Traditional solar cells have a limited trade between the series resistance, recombination losses, light absorption, efficiency, and high open-circuit voltages, as the electrical conduction and energy conversion occur on the front side. In IBC solar cells, these functions are independent of each other (Weimar, n.d.). Optical optimization is performed on the front surface, whereas electrical optimization focuses on the back side (Weimar, n.d.).

2.1 Concept

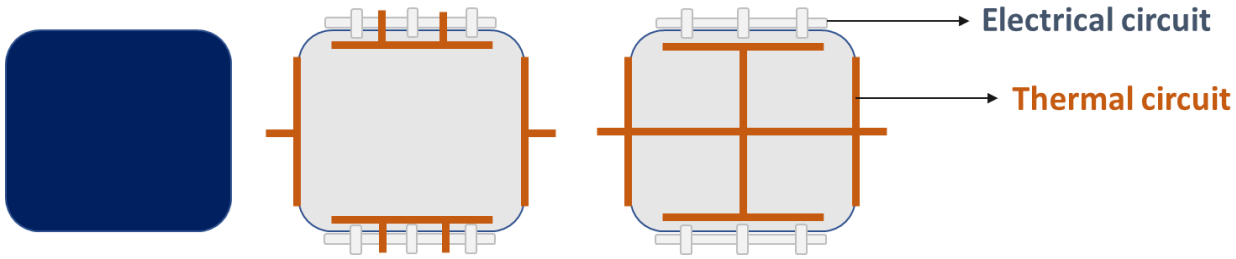

Figure 6- Concept for the design of a Thermal Circuit

An electrically insulated thermal circuit to be attached to the backside of the IBC cell to transfer the heat from the cell itself through the thermal circuit to the surrounding environment bypassing the EVA and Tedlar layer.

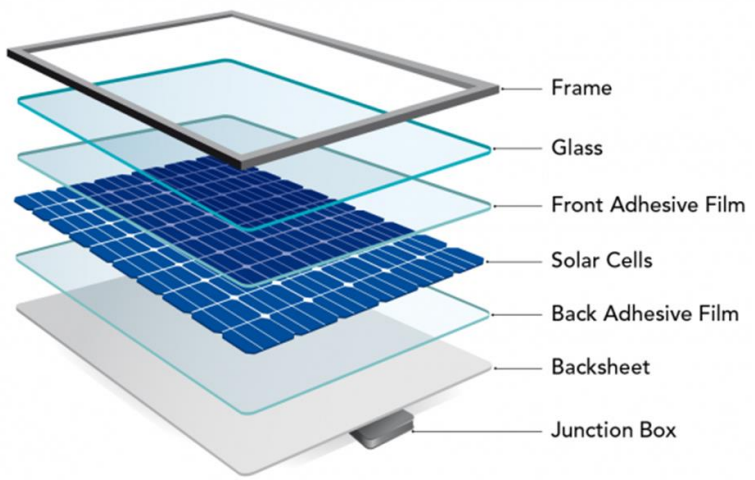

Figure 7- Layers that comprise a Solar Module (Miranda, 2022)

The thermal circuit is applied on a single IBC cell to check if the thermal circuit achieves proper electrical insulation. The IBC cell with the integrated heat sink is laminated, and its electrical properties are tested to ensure the cell is not compromised.

The compound material that insulates the thermal circuit is the Thermal Grizzly minus pad 8. The Thermal Grizzly contains modified silicon, is electrically insulating, and has very high thermal conductivity even with low contact pressure. The temperature range for the Thermal Grizzly is from -100◦C to 250◦C (minus pad 8, 2022) and thermal conductivity is 8 W/mK. Another option was using thermal paste; however, thanks to its high compressibility, the thermal pad was chosen as the final electrical insulator.

The research started with manufacturing a simple model of the integrated heat sink. Later, heat extraction studies were carried out to analyze the model cooling capacities, and later on, optimization of the model proceeded for a single cell.

Finally, the best-performing concept on the single-cell model was translated to a larger configuration of cells.

Some issues which might arise are a reduction in efficiency of the IBC solar cell due to the added thermal circuit, incomplete electrical insulation of the solar cell leading to a short circuit in the cell itself, or cracks reducing the lifetime and the performance of the solar panel.

2.2 Design

First, the tests started with a single solar cell to study how to add a thermal circuit into a conventional solar module, placing electrically insulating thermally conductive pads between the backside of the IBC solar cell and the EVA layer. The thermal pads were extruded at the edges of the solar cell to allow for conducting thin film metal strips to be added on top of them. This method ensures only heat is transferred from the IBC solar cell to the thin metal as the thermal pads act as an electrically insulating layer to avoid short-circuiting the cell.

The initial model for the thermal circuit was relatively simple as it was difficult to expect what the result from the lamination would be. Figure 8 presents the details of these first tests.

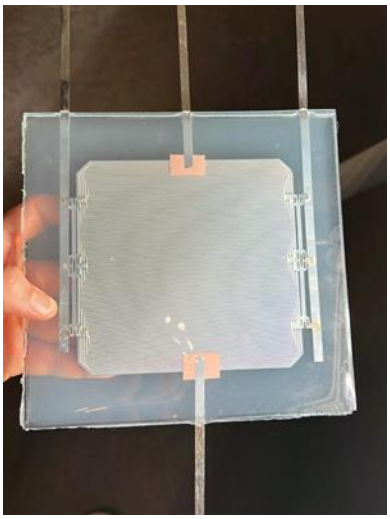

Figure 8- Backside view of Prototype 1

After successfully laminating the first solar cell without observing any cracks in the IBC solar cell, the cell was tested under a solar irradiance simulator to ensure the voltage and current output from the cell were unaffected and to ensure that no current or voltage was leaking from the newly added copper strips.

The rectangular pieces had an area of 2 cm2 and a thickness of 0.5 mm. They were located in the middle of both sides of a solar cell.

The prototype tests were under a solar irradiance generator, which provided around 970W/m2 of irradiance. The cell's voltage and current were measured and showed no irregularities. The current and voltage in the newly added metallic strips were also nonexistent, which was in coherence with expectations.

Prototype 2 and Prototype 3, as can be seen in figure 9a and figure 9b, were designed to check different variations of the thermal circuit to identify the most effective one.

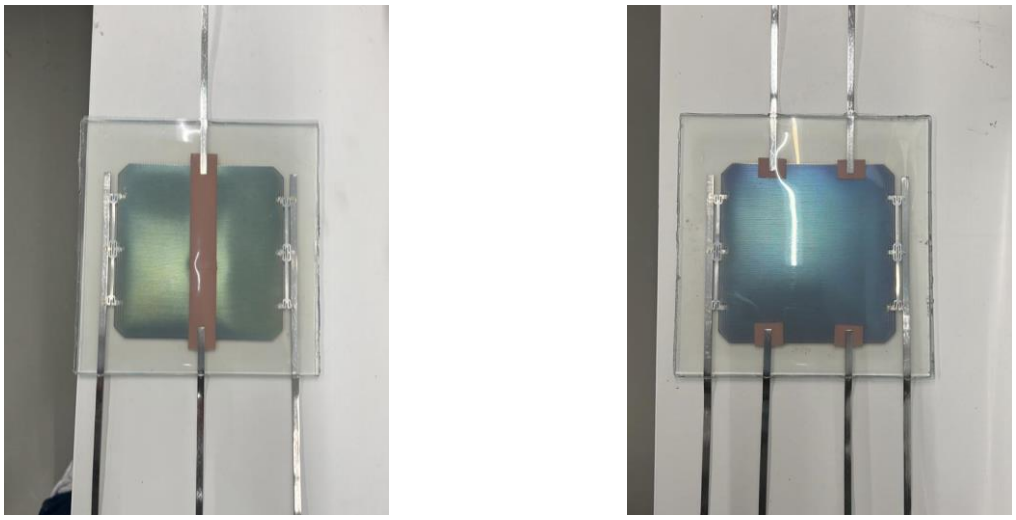

(a) (b)

Figure 9- a) Backside view of Prototype 2 (b) Backside view of Prototype 3

Tests were conducted to check the effectiveness of each prototype in extracting heat from the IBC solar cell.

A thermocouple was attached at the backside of each solar cell in addition to a simple IBC solar cell prototype with thermal tape. All solar cells were put under a solar simulator and were tested under a simulated light with wavelengths between 300 and 1200 nm, which ensures Pmax output (eternalsunspire, 2020). The Large Area Solar Simulator produces class AAA+ steady-state sunlight (eternalsunspire, 2020).

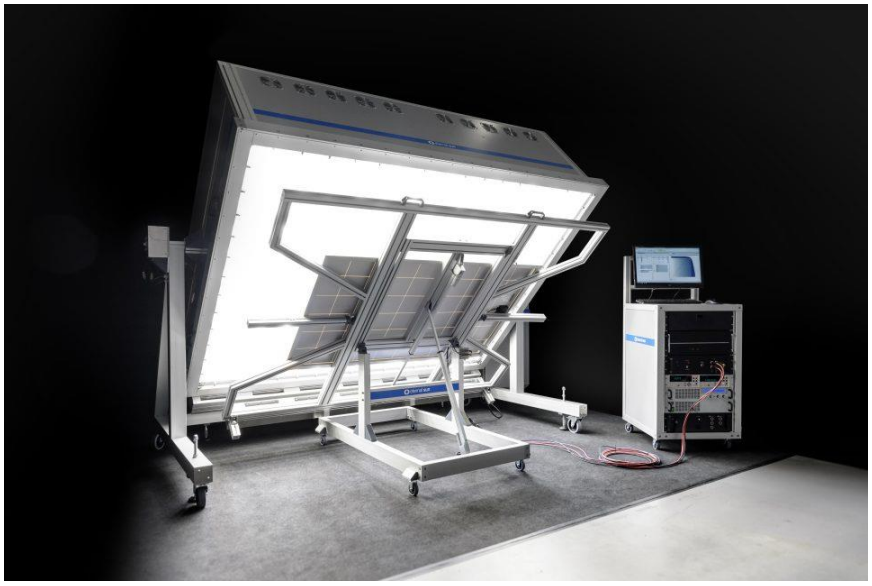

Figure 10- Large area Solar Simulator (LASS) (eternalsunspire, 2020)

2.3 Test

Test condition: Indoor testing

Test duration: 43 minutes

Continuous Irradiance: 18 minutes

Cooling without Irradiance: 25 minutes

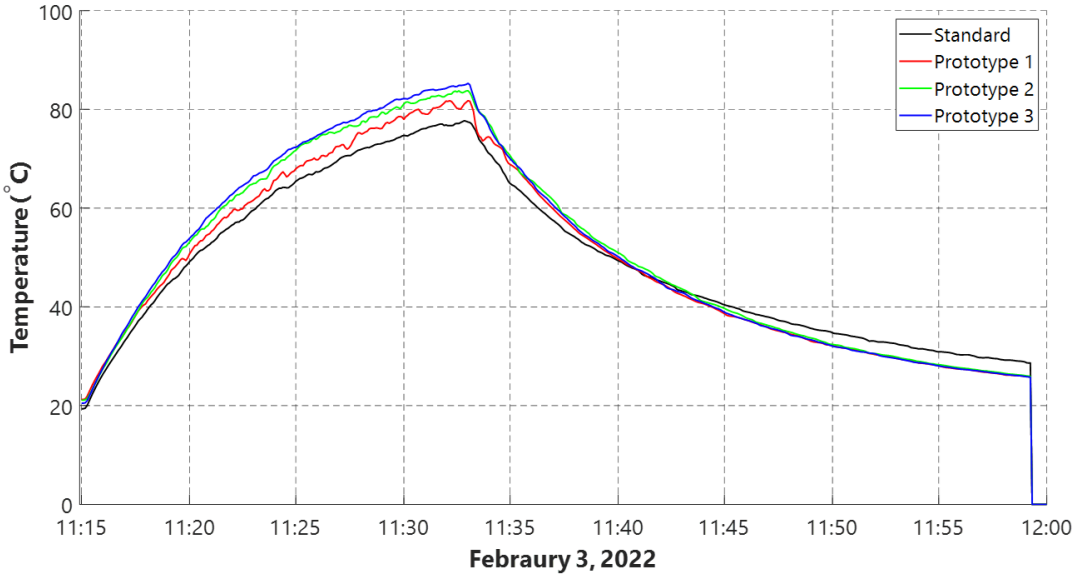

Figure 11- Testing Prototypes 1,2 and 3 under LASS February 3, 2022

2.3.1 Observations

It can be seen from the test that all prototypes absorbed heat instead of releasing it, as Prototype 3 achieved 85 °C the quickest, and the Standard cell with no heat sink had the lowest temperature throughout the test. It is also noteworthy that when the solar simulator was turned off, Prototype 3 experienced the fastest decrease in temperature and the Standard cell experienced the slightest decrease in temperature.

2.4 Remarks

Initially, the cell's temperature increase was thought to be from the newly integrated metal strips absorbing infrared radiation from the solar simulator and that it would operate properly in the external condition.

However, performing outdoor testing revealed the same results. Hence this increase may result from additional absorption of the metal. A larger thermal pad was used to improve heat extraction, and the copper metal strips were needed to absorb less infrared radiation. To this end, the front surface of the metal strips was covered by a piece of white Tedlar. A

white Tedlar also replaced the transparent Tedlar to reflect the unabsorbed light rays at the back of the PV cells.

2.5 Integrating Metals

The idea of adding a metal piece on top of the thermal pad was assessed to increase the heat transfer from the cell to the copper strip leading to the surrounding area. Different metals were considered, comparing the metal's specific heat capacity and thermal conductivity. In the end, copper was chosen due to its high thermal conductivity.

Table 3- Thermal properties of metals

	Thermal Conductivity (W/mK)	**Specific Heat Capacity (J/kg K)**
Aluminum	237.0	921.096
Copper	400.0	376.812
Lead	35.5	125.604
Tin	68.2	217.713

As a result of the different findings from the initial testing phase, a new set of prototypes was designed and manufactured to implement the new findings.

3 Prototypes

3.1 Generation 1- Prototypes

Prototypes 1 through 7 were created with varying thicknesses of the thermal pad and copper plate to understand how heat is transferred through the cell towards the integrated thermal circuit.

Table 4- Design specifications for Generation 1 prototypes

	Thermal Pad		**Copper plate**	
Prototypes	**Thickness (mm)**	**Surface Area (mm^2)**	**Thickness (mm)**	**Surface Area (mm^2)**
Prototype 1	0.5	100*100	0.5	65*65
Prototype 2	2	100*100	0.5	65*65
Prototype 3	0.5	100*100	NA	NA
Prototype 4	1	100*100	NA	NA
Prototype 5	2	100*100	NA	NA
Prototype 6	0.5	100*100	0.3	65*65
Prototype 7	0.5	100*100	0.5	65*65

All of the abovementioned prototypes have a single copper metal strip with a thickness of 0.3 mm and a width of 1 cm moving from the center of the strip towards the outside environment, and they contain a piece of white Tedlar covering the visible part of the metal.

Tests were performed underneath the solar simulator to understand how the various prototypes reacted to large amounts of heat.

3.1.1 Test 1

Test condition: Indoor testing

Test duration: 42 minutes

Continuous Irradiance: 9 minutes

Cooling without Irradiance: 33 minutes

Table 5- Temperature measurements for the indoor test performed on February 17, 2022

	Highest temperature achieved
Standard cell- Center	81.0°C
Standard cell- Edge	75.5°C
Prototype 1- Center	71.5°C
Prototype 1- Edge	68.0°C

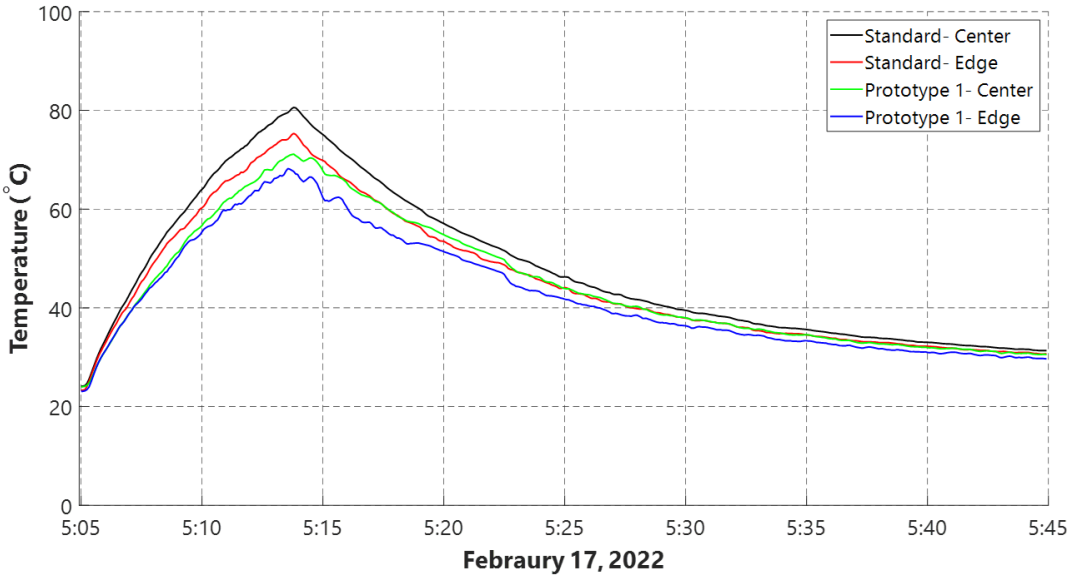

Figure 12-Testing Prototype 1 under LASS February 17, 2022

Observations

Temperature reduction achieved at the center of the cell is around 9.5 °C.

Temperature reduction achieved at the edge of the cell is around 7.5 °C.

Cooling was achieved faster in the Standard cell as the temperature difference between the Standard cell and Prototype 1 decreased during cooling for the exact locations.

3.1.2 Test 2

Test condition: Indoor testing

Test duration: 36 minutes

Continuous Irradiance: 14 minutes

Cooling without Irradiance: 22 minutes

Table 6- Temperature measurements for the indoor test performed on February 22, 2022

	Highest temperature achieved
Prototype 1- Center	74.8°C
Prototype 1- Edge	68.0°C
Prototype 2- Center	72.5°C
Prototype 2- Edge	69.0°C
Prototype 3- Center	83.0°C
Prototype 3- Edge	80.0°C

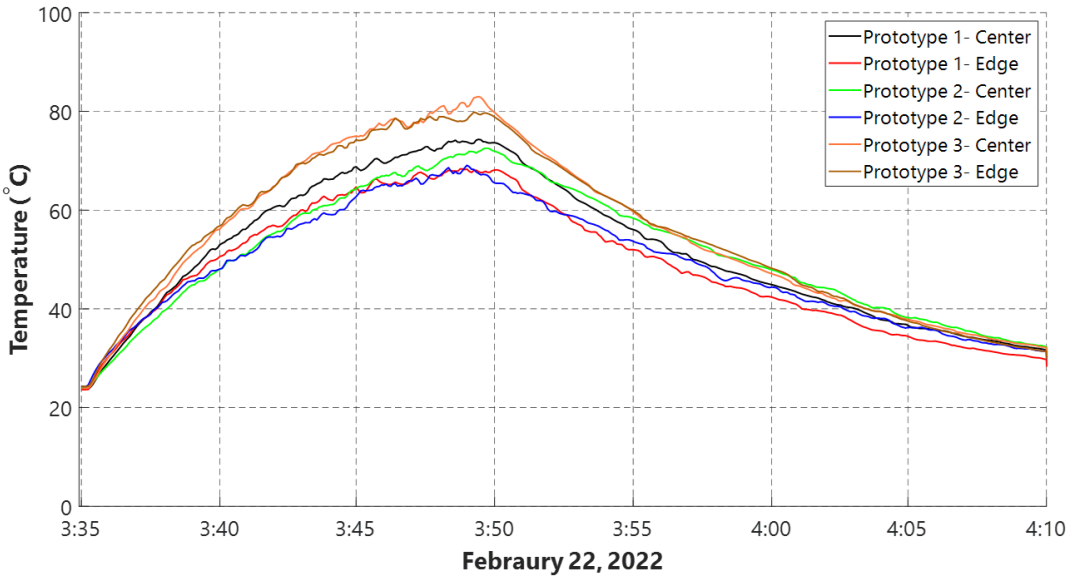

Figure 13- Testing Prototype 1,2 and 3 under LASS February 22, 2022

Observations

Prototype 2, with the thickest thermal pad and the copper layer, observed the cell's slowest temperature increase after turning on the solar simulator.

Prototype 3, which has the thinnest thermal pad, observed the cell's most significant temperature increase after turning on the solar simulator.

Prototype 3, with the thinnest thermal pad, observed the greatest decrease in temperature of the cell after turning off the solar simulator.

Prototype 2, with the thickest thermal pad and the copper layer, observed the lowest decrease in temperature of the cell after the solar simulator was turned off.

3.1.3 Test 3

Test condition: Outdoor testing

Test 3 was performed under real-time solar irradiance

Test duration: 60 minutes

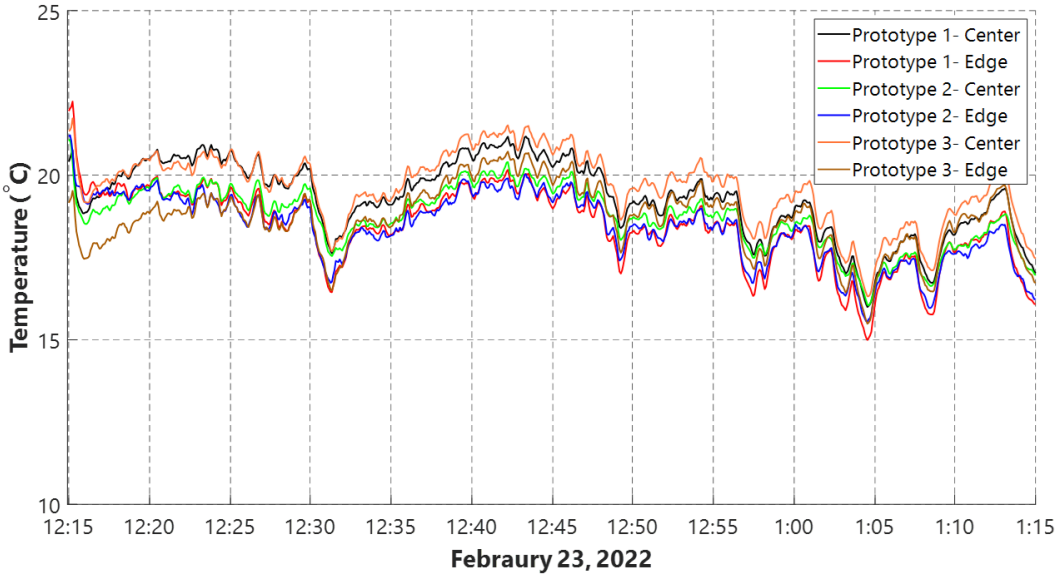

Figure 14- Outdoor testing of Prototypes 1,2 and 3 February 23, 2022

Observations

Although the temperature variation change was narrow, the same observations can be seen in Test 2, as Prototype 3 seems to have the highest temperature and Prototype 2 the lowest one.

Prototypes need to be insulated to see the effects of the newly added material.

To better understand which prototype was extracting the most heat, a thermocouple (Metal Edge) was placed on the backside of the metal strip leading outside, as seen in figure

15. The higher the temperature recording on the Metal Edge (ME), the higher the temperature extraction from the cell.

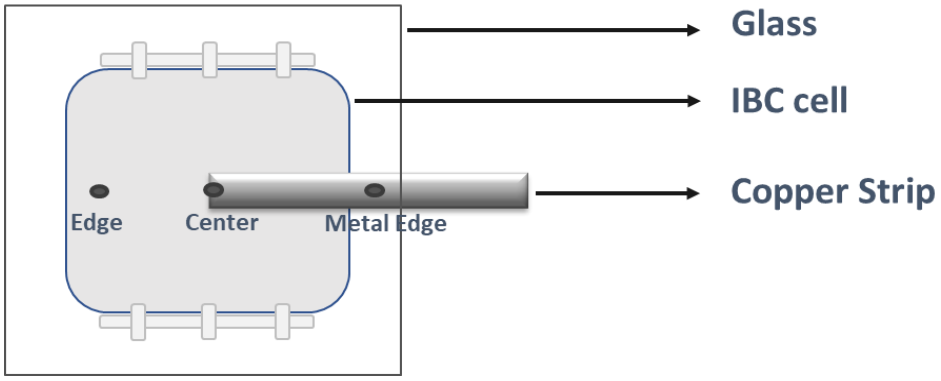

Figure 15- Positions of installed thermocouples

3.1.4 Test 4

Test condition: Indoor testing

Test duration: 35 minutes

Continuous Irradiance: 8 minutes

Cooling without Irradiance: 29 minutes

Table 7-Temperature measurements for the indoor test performed on March 2, 2022

	Highest temperature achieved
Prototype 3- Edge	81.0°C
Prototype 3- Metal Edge	72.5°C
Prototype 4- Edge	75.5°C
Prototype 4- Metal Edge	65.0°C
Prototype 5- Edge	75.5°C
Prototype 5- Metal Edge	65.0°C
Prototype 6- Edge	80.0°C
Prototype 6- Metal Edge	65.0°C

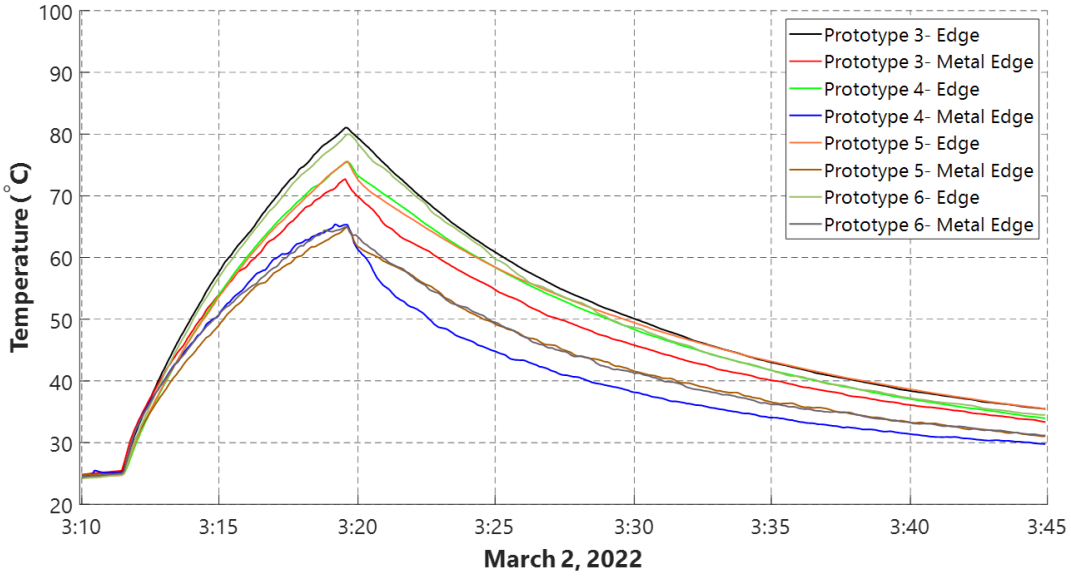

Figure 16- Testing Prototypes 3,4,5 and 6 under LASS March 3, 2022

Observations

Prototype 3, having the thinnest heat pad and no copper plate, has the highest capacity to extract heat because its temperature at the ME was the highest, meaning that more heat travels from the cell through the thin copper strip.

Prototype 3 also experienced the highest amount of heating of the cell.

Prototype 4 and Prototype 5, having only a thermal pad of 1 mm and 2 mm, respectively, showed similar responses during heating and cooling, following almost identical temperature profiles. However, Prototype 4 with the thinner heat sink showed faster cooling.

Prototype 6 was superior to Prototype 3 in heat extracting capacity as the temperature difference recorded at ME was around 7.5°C higher for Prototype 3 than for Prototype 4, meaning that the addition of a copper plate in the middle of the cell decreased the heat extracting capacity.

3.1.5 Test 5

Test condition: Indoor testing

Test duration: 20 minutes

Continuous Irradiance: 10 minutes

Cooling without Irradiance: 10 minutes

Table 8-Temperature measurements for the indoor test performed on March 2, 2022

	Highest temperature achieved
Prototype 6- C	72.5°C
Prototype 6- E	73.0°C
Prototype 6- ME	68.0°C
Prototype 7- C	73.0°C
Prototype 7- E	75.0°C
Prototype 7- ME	64.5°C

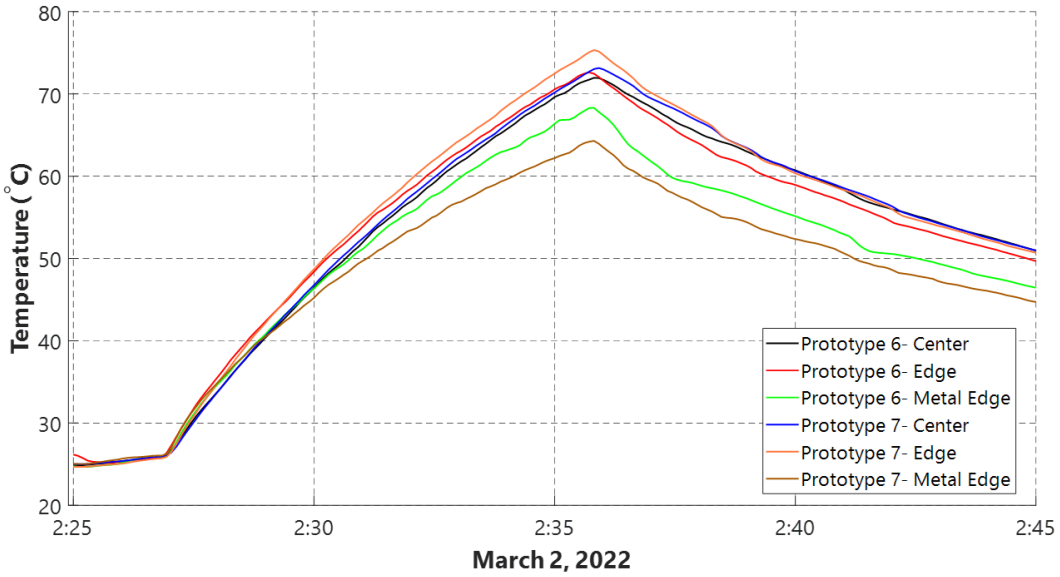

Figure 17- Testing Prototypes 6 and 7 under LASS March 2, 2022

Observations

Prototype 6 performed better in extracting heat as the temperature recorded at the edge of Prototype 6 is lower than the temperature recorded on Prototype 7. Moreover, the temperature recorded on the metal edge is higher for Prototype 6 than for Prototype 7, meaning that more heat goes from the cell itself toward the surrounding.

3.1.6 Test 6

Test condition: Outdoor testing

Test duration: 25 minutes

Figure 18- Setup configuration of prototypes with tape insulation on the sides

Edges of the cell were insulated, leaving the backside of the cells exposed, leaning on the wall, as shown in figure 18. The Standard cell was tested alongside Prototype 3, which proved to be the best performing cell in heat extraction under the solar simulator.

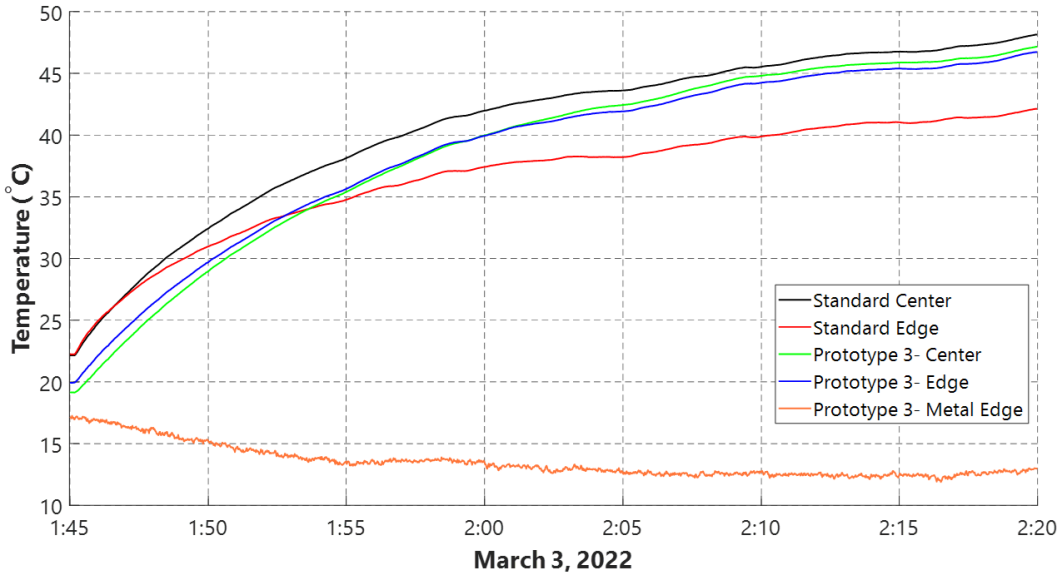

Figure 19- Outdoor testing of prototype March 3, 2022 (1)

Observations

The smooth curves attest to the proper insulation of the edges of the cells and the thermocouples.

Prototype 3 performed worse than the Standard cell as the temperature recorded at the edge of the Standard cell was lower than the temperature recorded at the edge of Prototype 3.

The temperature at the center of Prototype 3 is lower than at the center of the Standard cell, which is most likely the result of the added thermal pad layer in the cell.

3.1.7 Test 7

Test condition: Outdoor testing

Test duration: 55 minutes

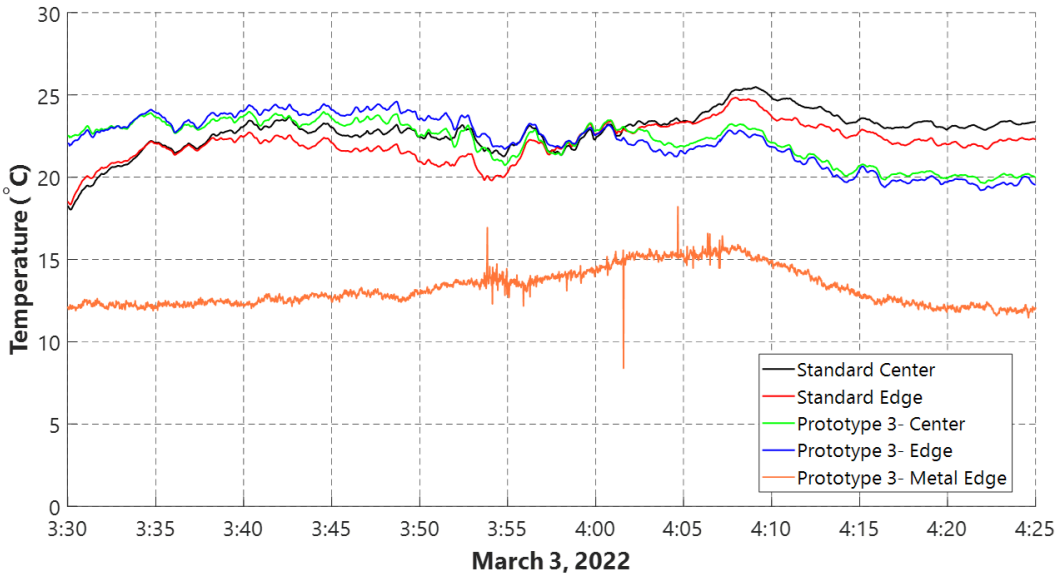

Figure 20-Outdoor testing of prototype March 3, 2022 (2)

Observations

At around 4:00 pm, the position of the cells was modified, leading to a variation in the temperature readings of the cells, where the Standard cell had a lower cell temperature in the first position and Prototype 3 had a lower cell temperature in the second position.

3.1.8 Remarks

The thickness of the heat pad or the copper plate influences the heat flow towards the outside environment. The thinner the heat pad and the copper, the more heat can be extracted. However, the additional thickness allows for the lower temperature of the cell itself under continuous heating since more heat can be absorbed and stored in the additional layers of thickness.

Further improvements were necessary to produce better prototypes. A better understanding of the thermal pad and copper plate size is needed to understand its effect on heat extraction.

The position of the prototypes needs to be improved while testing to ensure equal sun and wind exposure.

3.2 Generation 2- Prototypes

Generation 2 prototypes aimed to study the effect of narrower thermal pads on the heat extraction capacity of the cells.

Table 9- Design specifications for Generation 2 prototypes

	Thermal Pad		**Copper plate**	
Prototypes	**Thickness (mm)**	**Surface Area (mm^2)**	**Thickness (mm)**	**Surface Area (mm^2)**
Prototype 1A	0.5	30*120	NA	NA
Prototype 2A	0.5	30*120	NA	NA
Prototype 3A	0.5	30*120	NA	NA

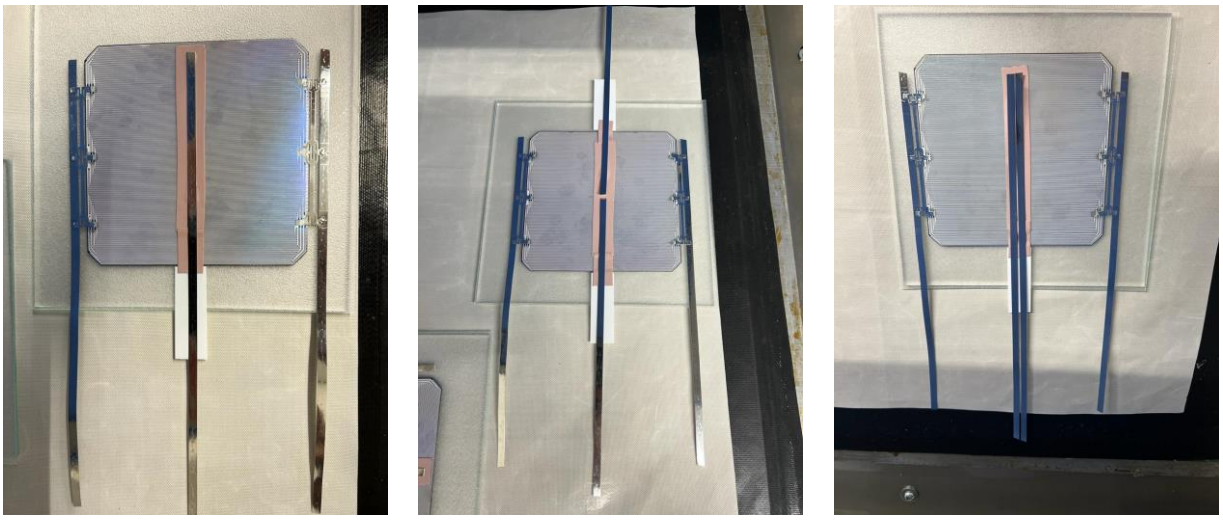

(a) (b) (c)

Figure 21- a) Backside view of Prototype 1A b) Backside view of Prototype 2A c) Backside view of Prototype 3A

3.2.1 Test 1

Test condition: Indoor testing

Test duration: 30 minutes

Continuous Irradiance: 10 minutes

Cooling without Irradiance: 20 minutes

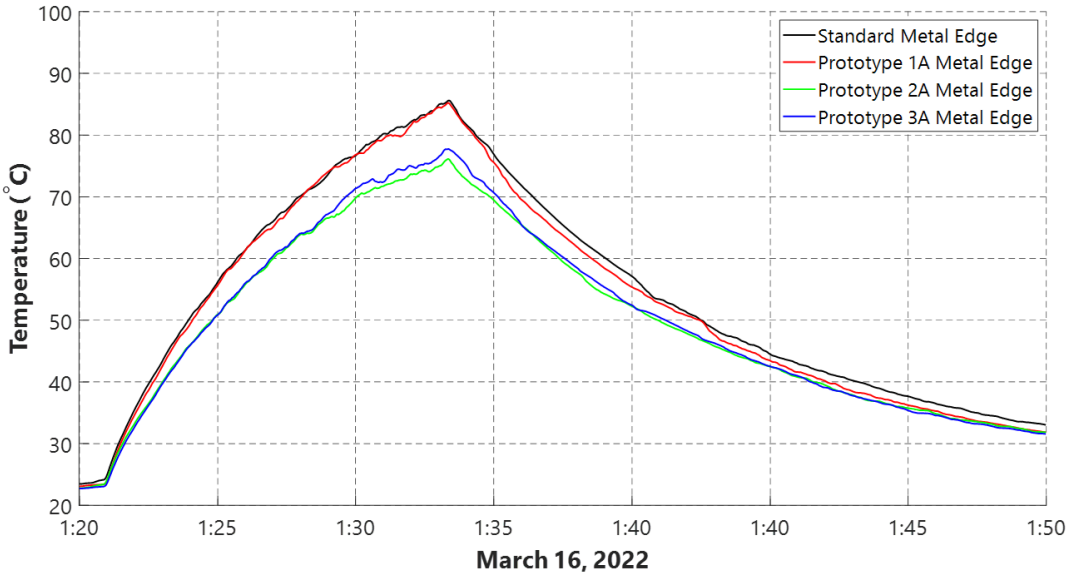

Figure 22- Testing Prototypes 1A,2A, and 3A under LASS March 16, 2022

Observations

Prototype 2A and Prototype 3A had similar performance as it can be seen that by adding two copper strips, the heat is divided between two paths, lowering the temperature reading on each strip.

Prototype 1 had the highest temperature reading on the metal edge among the three prototypes; hence in a single copper strip, the most heat was extracted.

3.3 Generation 3- Prototype

Generation 3 prototypes aimed to study the effect of increasing the copper strip width, leading to the outside environment, on the heat extraction capacity of the cells.

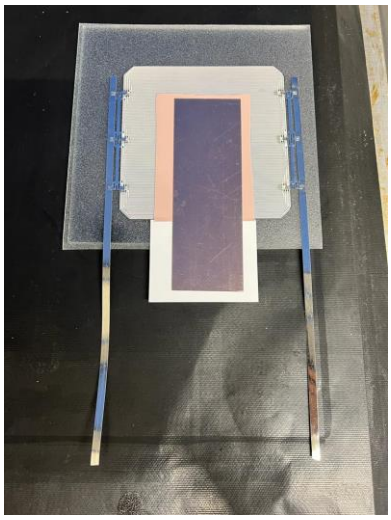

Figure 23- Backside view of Prototype 1B

Table 10- Design specifications for Generation 3 prototype

	Thermal Pad		Copper plate	
Prototypes	**Thickness (mm)**	**Surface Area (mm^2)**	**Thickness (mm)**	**Surface Area (mm^2)**
Prototype 1B	0.5	70*100	0.3	50*150

Figure 24- Setup for test procedure on March 24, 2022

3.3.1 Test 1

Test condition: Outdoor testing

Test duration: 1 hour 45 minutes

All thermocouples were placed in the center of the prototypes.

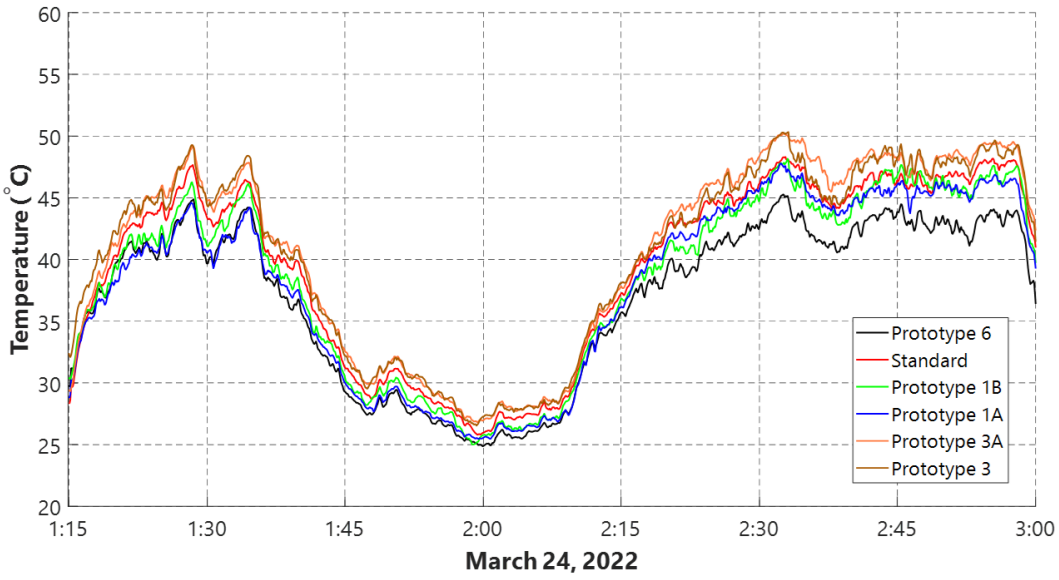

Figure 25- Outdoor testing of Prototypes 3,6,1A,1B,3A March 24, 2022

Observations

Prototype 6 performed the best as it recorded the lowest temperature among all tested prototypes. Prototype 1B also performed well as it recorded the second-lowest temperature reading.

3.3.2 Test 2

Test condition: Outdoor testing

Test duration: 1 hour 45 minutes

Test 2 was performed to confirm the result found the previous day in Test 1. For this test, the positions of the cells within the fabricated mini-module were altered to confirm that changing the position of the cells would have minimal impact on the results.

All thermocouples were placed in the center of the prototypes.

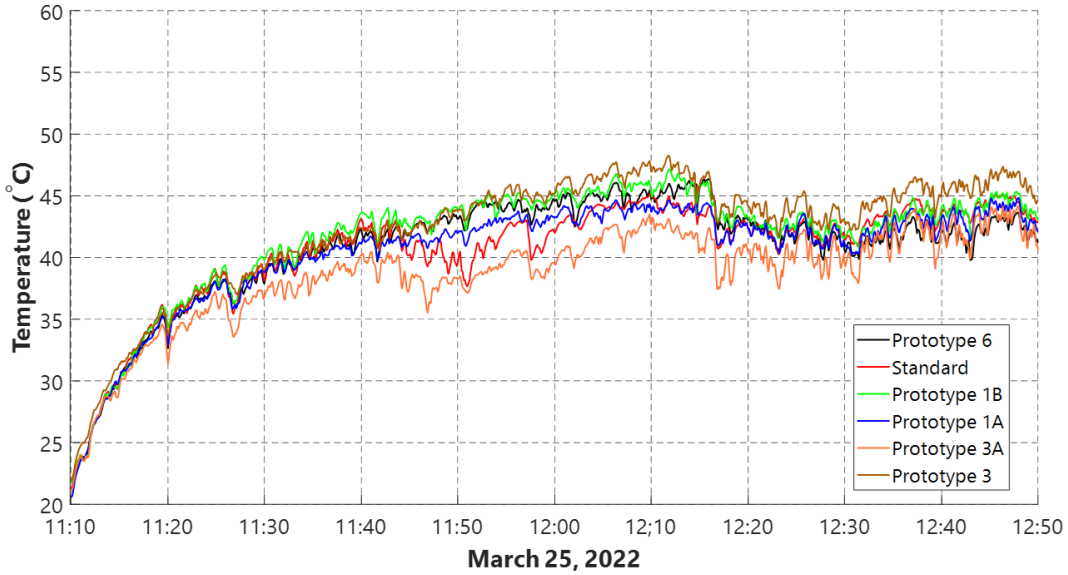

Figure 26-Outdoor testing of Prototypes 3,6,1A,1B,3A March 25, 2022

Observations

None of the best performing cells of Test 1 had the same performance in Test 2. The position of the cells still had a significant influence on the outcome of the test.

3.3.3 Test 3

Test condition: Outdoor testing

Test Duration: 2 days

Present in the graph is the most representative day to make sure the data is comprehensible.

Setup: All prototypes were placed horizontally next to one another and fixed at the top and bottom with aluminum frames on the mounting station (see figure 24), and directed towards the south at an angle of 30 degrees.

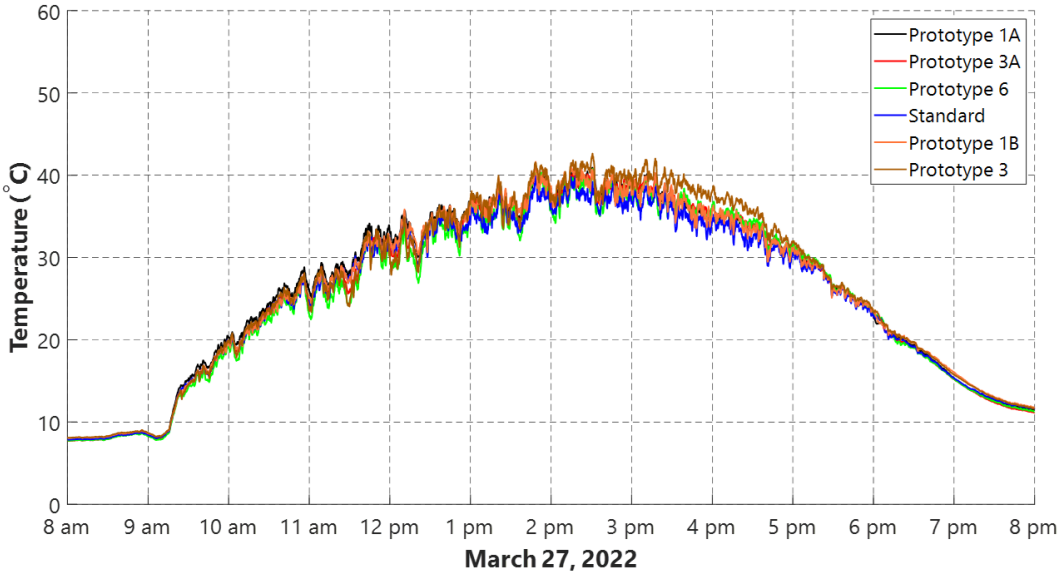

Figure 27- Outdoor testing of Prototypes 3,6,1A,1B,3A March 27, 2022

Observations

All cells performed worse in terms of heat extraction than the Standard cell. Prototype 6 performed better until around 1 pm; however, it was later overtaken by the Standard cell. Some reasons might be inconsistent wind patterns on the backside of different cells. Another reason might be that the amount of thermal pad and copper covering the backside surface of the PV cell was reducing the capacity of natural convection to extract heat more than it was assisting in extracting heat. Another reason might be that the exposed part of the copper behind the Tedlar transferring heat from the cell to the surrounding absorbs heat through direct irradiance from the sun, hence increasing the cell's temperature.

3.3.4 Remarks

Test some material that may reflect more direct sunlight from the copper strip underneath the exposed part of the Tedlar.

Cover the edges and increase the width and thickness of the metal, extracting the heat to reduce the material's thermal resistance compared to natural convection.

3.4 The reflectance of Materials & Thermal Resistivity

3.4.1 Reflectance of Materials

Different materials were evaluated to see how the increased operating temperature produced by the absorbed irradiance on the exposed copper strip could be reduced. The most interesting of which was aluminum foil.

The aluminum foil's light reflection ability is powerful. Its light reflectivity is affected by the purity, smoothness, surface roughness, heat-ray wavelength, and other factors. Increasing the purity and heat ray wavelength of the aluminum foil, the light reflectance increases, and with the decrease of the flatness and surface roughness, the light reflectivity of aluminum foil decreases. In the visible wavelength range of 380-765 nm, the reflectivity is about 70% – 80%, and in the infrared wavelength scope of 760 nm to 1000 nm, the reflectivity can reach 75%- 100% (Nydia, 2017).

3.4.2 Thermal Resistivity

$$R_{original} = R_{EVA} + R_{Tedlar}$$

$$R_{new} = (R_{new_1} * R_{new_2})/(R_{new_1} + R_{new_2})$$

$$R_{new_1} = R_{EVA} + R_{Tedlar}$$

$$R_{new_2} = R_{Thermal\ pad} + R_{copper-parallel} + R_{copper-perpendicular}$$

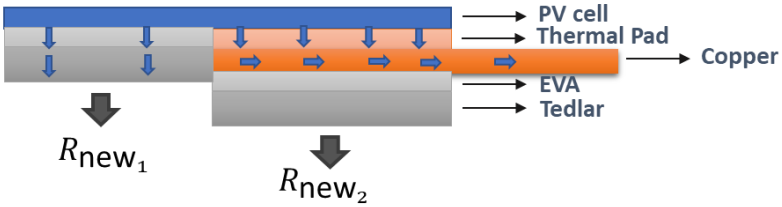

Figure 28- Illustration of heat flow for a standard cell and a modified cell

$$R = \frac{\Delta x}{A.\kappa}$$

R= Thermal resistance across the sample (K/W)

Δx= Thickness parallel to the heat flow (m)

A= Cross-sectional area perpendicular to heat flow (m^2)

κ= Thermal conductivity of the material $(W/(K.m))$

Achieving effective cooling means the heat must flow through the thermal pad towards the metal and the surrounding environment. This arrangement will prevent the heat from

passing from the IBC solar cell towards the EVA layer, the Tedlar, and finally towards the environment.

To achieve this, the thermal resistivity of the new path should be lower than the thermal resistivity of the same path in the normal cell.

The path the heat has to travel horizontally through the copper strip is the limiting factor of the internal heat sink design since it has the highest thermal resistivity due to the significant distance over area factor. To improve the thermal resistivity of this path, a thicker copper would help improve the heat transfer, and a shorter distance by which heat travels from the cell towards the outside surrounding would also improve thermal resistivity.

Original thermal resistance for the part of the cell to be covered by thermal pad and copper:

$$R_{original} = R_{EVA} + R_{Tedlar}$$

$$R_{original} = (\frac{\Delta x}{A.\kappa})_{EVA} + (\frac{\Delta x}{A.\kappa})_{Tedlar}$$

New thermal resistance for the cell having additional thermal pad and copper:

$$R_{\text{new}} = (R_{\text{new}_1} * R_{\text{new}_2})/(R_{\text{new}_1} + R_{\text{new}_2})$$

$R_{\text{new}_1} = R_{\text{EVA}} + R_{\text{Tedlar}}$

$R_{\text{new}_2} = R_{\text{Thermal pad}} + R_{\text{copper-parallel}} + R_{\text{copper-perpendicular}}$

3.5 Generation 4- Prototypes

Generation 4 prototypes were created with the thermal resistance considerations in mind, hence a shorter path for the heat to cross through the copper strip and a thicker copper strip.

Table 11- Design specifications for Generation 4 prototypes

	Thermal Pad		**Copper plate**	
Prototypes	**Thickness (mm)**	**Surface Area (mm^2)**	**Thickness (mm)**	**Surface Area (mm^2)**
Prototype 1C	0.5	8*120	0.5	8*120
Prototype 2C	0.5	16*120	0.5	16*120
Prototype 3C	0.5	8*120	0.3	8*120

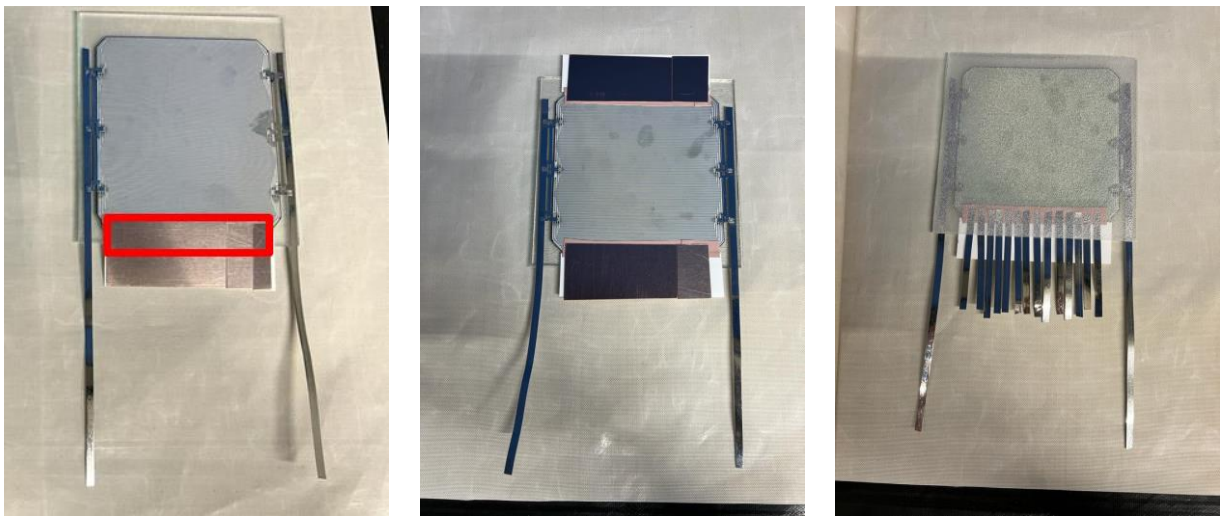

(a) (b) (c)

Figure 29- a) Backside view of Prototype 1C b) Backside view of Prototype 2C c) Backside view of Prototype 3C

3.5.1 Thermal Resistivity improvement in Prototype 1C

The thermal Conductivity of EVA is taken as 0.34 W/mk (Ethylene Vinyl Acetate (EVA), 2020).

The thermal Conductivity of the Tedlar is taken as 0.2 W/mk (Oh, et al., 2018).

The thickness of the EVA was measured in the lab to be 0.4mm.

The thickness of the Tedlar was measured in the lab to be 0.5mm.

$$R_{original} = R_{EVA} + R_{Tedlar}$$

$$R_{original} = \left(\frac{0.4 * 10^{-3}}{0.34 * 12.5 * 10^{-2} * 12.5 * 10^{-2}}\right)_{EVA} + \left(\frac{0.5 * 10^{-3}}{0.2 * 12.5 * 10^{-2} * 12.5 * 10^{-2}}\right)_{Tedlar}$$

$$R_{original} = (1.3)_{EVA} + (2.368)_{Tedlar}$$

$$R_{original} = 0.2353 K/W$$

$$R_{new_1} = \left(\frac{0.4 * 10^{-3}}{0.34 * 12.5 * 10^{-2} * (12.5 - 0.85) * 10^{-2}}\right)_{EVA} + \left(\frac{0.5 * 10^{-3}}{0.2 * 12.5 * 10^{-2} * (12.5 - 0.85) * 10^{-2}}\right)_{Tedlar}$$

$$R_{new_1} = (0.0807)_{EVA} + (0.1717)_{Tedlar}$$

$$R_{new_1} = 0.2524 K/W$$

$$R_{new_2} = R_{Thermal\ pad} + R_{copper-parallel} + R_{copper-perpendicular}$$

$$R_{new_2} = \left(\frac{0.5 * 10^{-3}}{8 * 10 * 10^{-2} * 0.85 * 10^{-2}}\right)_{Thermal\ pad} + \left(\frac{0.3 * 10^{-3}}{356 * 10 * 10^{-2} * 0.85 * 10^{-2}}\right)_{copper-parallel} + \left(\frac{(0.85 + 0.4) * 10^{-2}}{356 * 0.3 * 10^{-3} * 10 * 10^{-2}}\right)_{copper-perpendicular}$$

$$R_{new_2} = (7.35 * 10^{-2})_{Thermal\ pad} + (9.914 * 10^{-4})_{copper-parallel} + (1.17)_{copper-perpendicular}$$

$$R_{new_2} = 1.2445 K/W$$

$$R_{\text{new}} = (R_{\text{new}_1} * R_{\text{new}_2})/(R_{\text{new}_1} + R_{\text{new}_2})$$

$$R_{\text{new}} = (0.2524 * 1.2445)/(0.2524 + 1.2445)$$

$$R_{\text{new}} = 0.20984 K/W$$

The thermal resistivity of Prototype 1C improved by around 11%. Thanks to the modified section of the cell, from 0.2353K/W to 0.20984K/W.

3.5.2 Test 1

Test condition: Indoor testing

Test duration: 45 minutes

Continuous Irradiance: 13 minutes

Cooling without Irradiance: 32 minutes

All thermocouples were placed in the center of the prototypes.

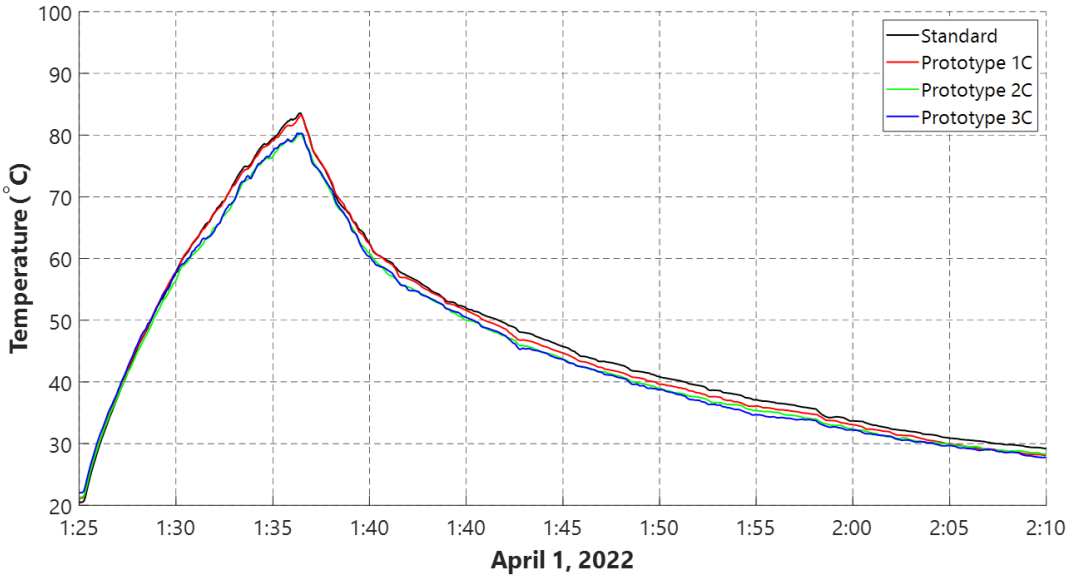

Figure 30- Testing Prototypes 1C,2C and 3C under LASS April 1, 2022 (1)

Observations

Prototype 2C and Prototype 3C performed the best as they had the lowest temperature. However, a temperature reduction of 2°C was observed, whereas Prototype 1C performed almost identically to the Standard cell.

3.5.3 Test 2

Test condition: Indoor testing

Test duration: 37 minutes

Continuous Irradiance: 10 minutes

Cooling without Irradiance: 27 minutes

Setup: Styrofoam was used to block irradiance from the solar simulator reaching the exposed part of the copper strip underneath the Tedlar.

All thermocouples were placed in the center of the prototypes.

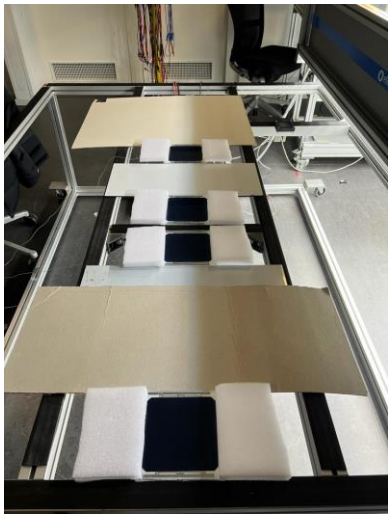

Figure 31- Setup for test procedure on April 1, 2022 (2)

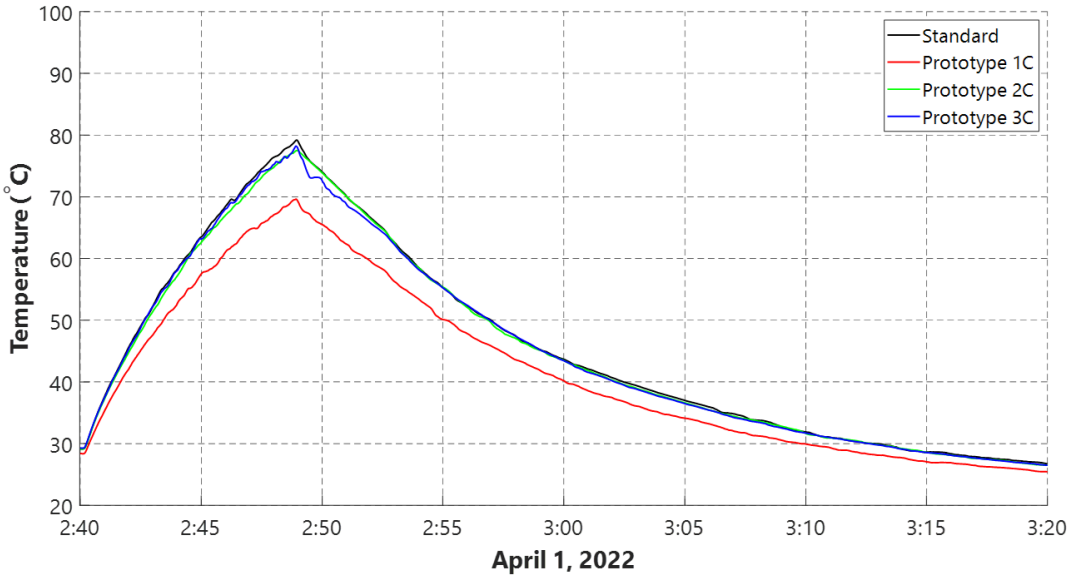

Figure 32- Testing Prototypes 1C,2C and 3C under LASS April 1, 2022 (2)

Observations

No improvements in temperature reduction were observed when the Styrofoam was added to the Prototypes.

3.5.4 Test 3

Test condition: Indoor testing

Test duration: 35 minutes

Continuous Irradiance: 10 minutes

Cooling without Irradiance: 25 minutes

Setup: Cardboard tape was used to block irradiance from the solar simulator reaching the exposed part of the copper strip underneath the Tedlar.

All thermocouples were placed in the center of the prototypes.

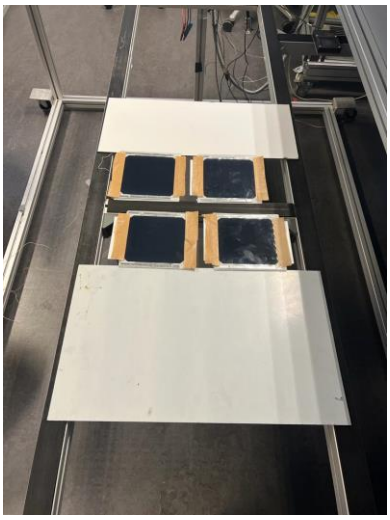

Figure 33-Setup for test procedure on April 1, 2022 (3)

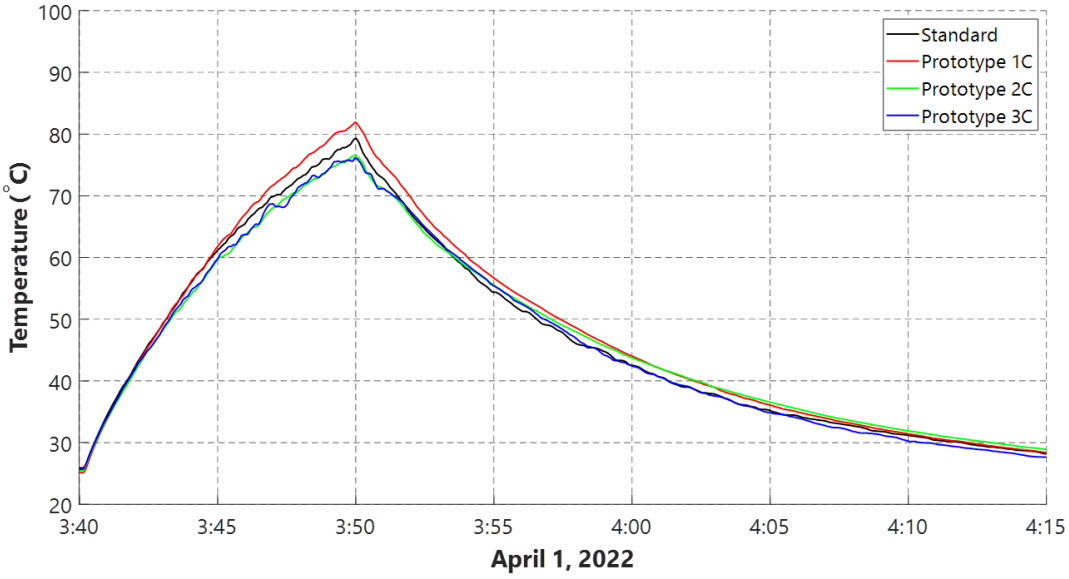

Figure 34-Testing Prototypes 1C,2C and 3C under LASS April 1, 2022 (3)

Observations

No improvements in temperature reduction were observed when the cardboard tape was added to the Prototypes.

3.5.5 Remarks

The indoor solar simulator is not a suitable testing site for the models with large copper strips as it raises the surrounding ambient temperature significantly, not allowing the copper strips to cool down as they would in an outdoor environment.

3.6 Generation 5- Prototypes

Generation 5 prototypes are the same as the generation 4 prototypes. The only variation is using aluminum as a conducting metal instead of copper.

The reason behind the creation of prototypes using aluminum, although the conductivity of copper is comparatively higher, was that aluminum had a higher reflectivity. Aluminum would reflect more irradiance incidents from the sun compared to copper. Moreover, aluminum also has a higher thermal capacity, meaning it can withstand higher amounts of heat before its temperature changes by a single degree.

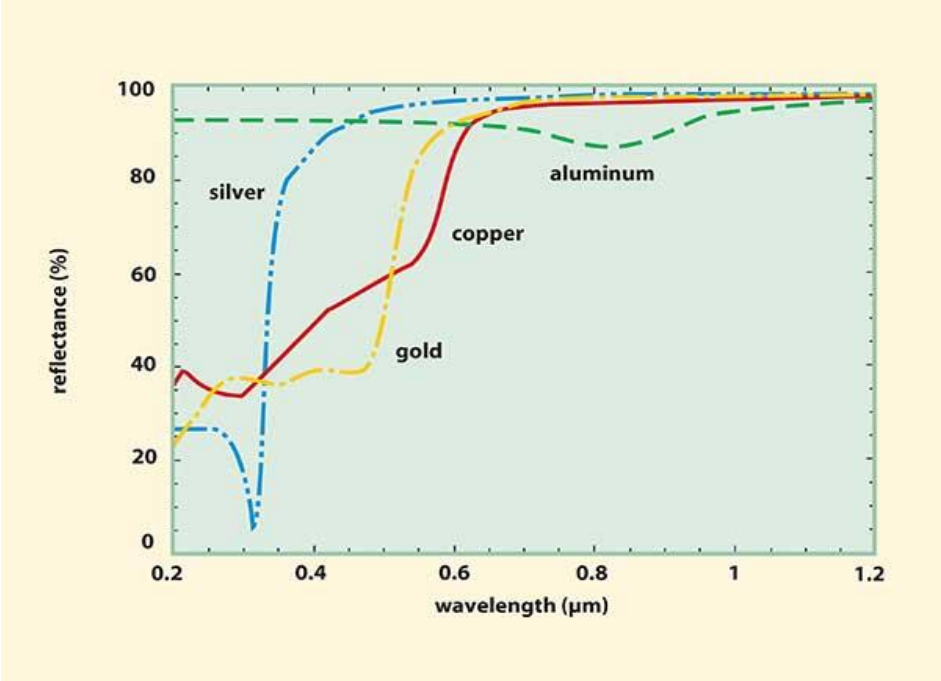

Figure 35-The reflectance of several shiny metals vs. wavelength from 0.2 to 1.2 μm, taken from (Photonics, n.d.)

Table 12- Design specifications for Generation 5 prototypes

	Thermal Pad		**Aluminum plate**	
Prototypes	**Thickness (mm)**	**Surface Area (mm^2)**	**Thickness (mm)**	**Surface Area (mm^2)**
Prototype 1D	0.5	8*120	0.5	8*120
Prototype 2D	0.5	16*120	0.5	16*120

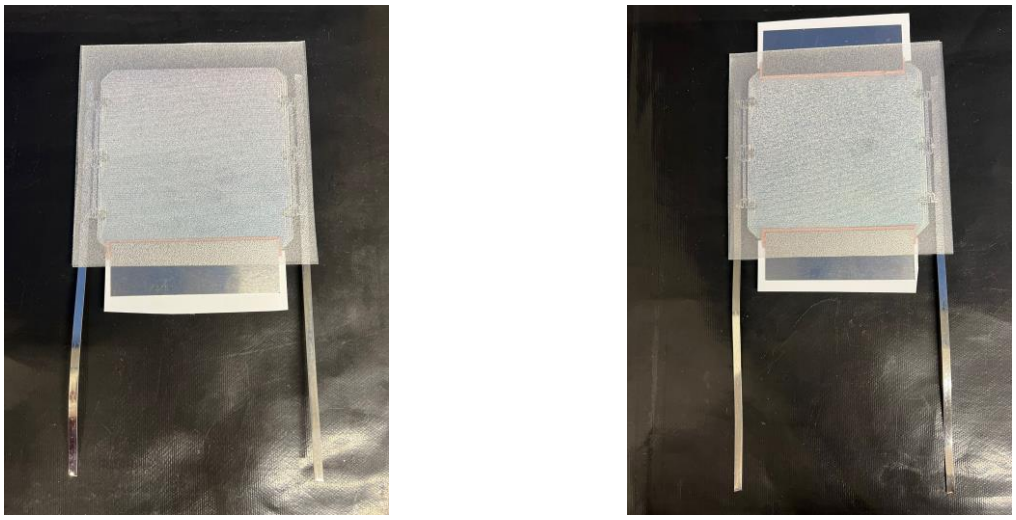

(a) (b)

Figure 36- a) Backside view of Prototype 1D b) Backside view of Prototype 2D

3.6.1 Test 1

Test condition: Outdoor testing

Test duration: 1 hour 35 minutes

All thermocouples were placed in the center of the prototypes.

Observations

After 1 pm, the thermocouple attached to the Standard cell disconnected, hence the lower temperature reading compared to the other cells.

Prototype 2C performed better than Prototype 1C, and Prototype 2D performed better than Prototype 1D, which meant that having copper or aluminum on both sides of a solar cell increases the amount of heat that can be extracted from a cell, leading to lower temperature readings than having copper or aluminum on one side only. This "added" heat extraction could be because of the added symmetry, making the solar cell distribute the heat more evenly, or it could be due to more heat extraction.

Prototype 1C and Prototype 1D performed almost identically, Prototype 2C and Prototype 2D performed almost identically, with Prototype 2C and Prototype 2D performing marginally better than their counterparts, asserting that copper is better for heat extraction due to its high conductivity.

The Standard cell still had the lowest temperature among all the tested cells, this could be due to the low convection on the metal strips outside the cells, or it could be due to the low amount of heat transferred from the cell as a result of a small area of contact between the cell and the thermal pad.

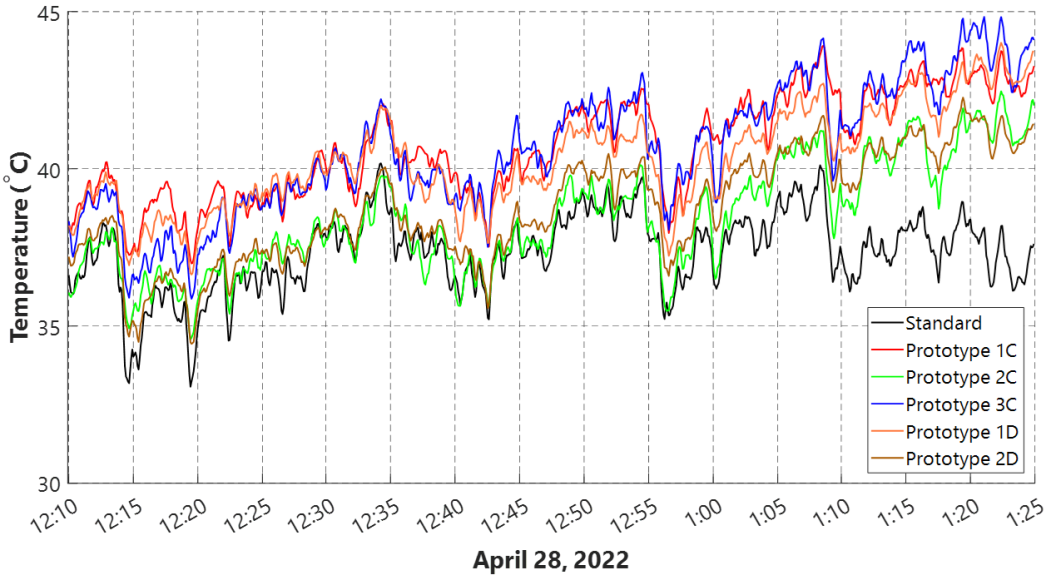

Figure 37-Outdoor testing of Prototypes 1C,2C,3C,1D and 2D April 28, 2022

3.6.2 Test 2

Test condition: Outdoor testing

Test duration: 1 hour

All thermocouples were placed in the center of the prototypes.

To determine if aluminum foil could help reflect the sunlight and reduce absorption in the part of the aluminum/copper underneath the glass and away from the cell itself, aluminum tape was used to cover the top glass over the metals.

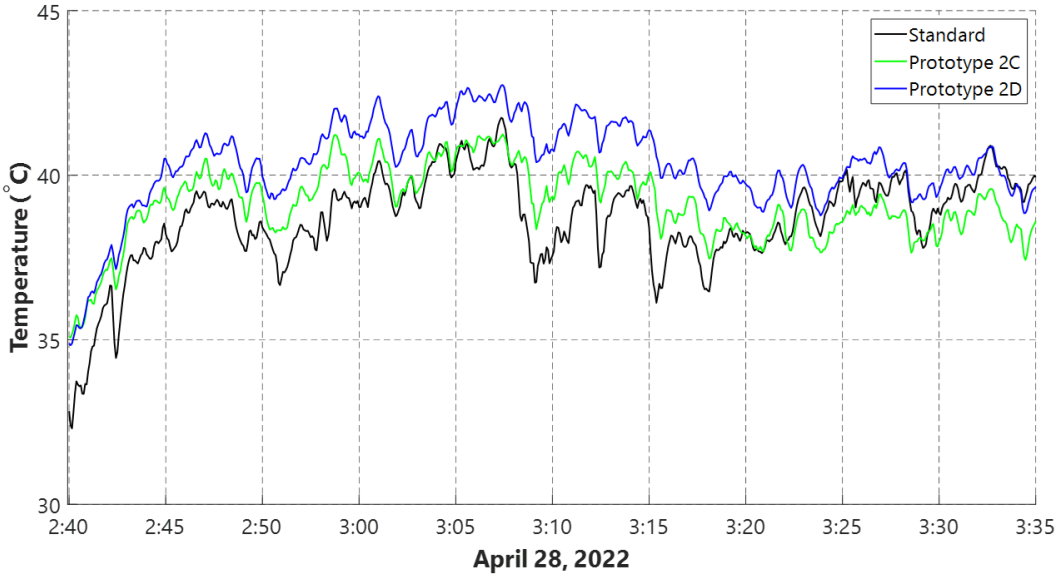

Figure 38-Outdoor testing of Prototypes 2C and 2D April 28, 2022

Observations

Both prototypes performed worse when using the aluminum tape to cover the top of the metal visible through the glass. This performance change could be due to the aluminum tape potentially reducing the amount of convection on the glass, leading to higher temperatures.

3.6.3 Remarks

Copper is marginally better than aluminum in heat extraction capabilities. The higher heat capacity and higher reflectivity of aluminum were thought to give it the edge in the heat extraction application; however, copper proved to be the better option.

Increasing the heat transfer from the cell to the thermal pad and copper strip is needed to increase temperature reduction.

Aluminum foil, Cardboard tape, and Styrofoam all have an insignificant effect on the temperature performance of the cells by blocking incoming irradiance from the sun. In some cases, they could even have a negative effect by decreasing convection on the surface of the glass, leading to an increase in temperature in the cell.

3.7 Optimizing design using Matlab

A Matlab code was created to estimate the exact length needed on the thermal pad and copper to improve cooling.

3.7.1 Matlab Function Logic

The code calculates the thermal resistivity of the standard solar cell without any modifications, taking into account that the heat transferred from the cell to the EVA layer, then to the Tedlar, and finally to the surrounding environment. After calculating the original thermal resistivity of the cell, the code estimates a new thermal resistivity considering the thermal pad and the copper. The purpose is to direct some of the heat from the cell through the new circuit toward the environment. The code starts by assuming that the thermal pad and copper strip cover 1 mm of the cell. Later on, by iterations of length with a resolution of 0.1 mm, new values of the thermal resistivity are estimated. Then the modified cell having an indentation with a thermal resistivity equal to the original cell's thermal resistivity is considered the optimal design. The code is designed in such a way to find the maximum indentation possible without increasing the thermal resistivity compared to the original cell. This decision is because it was found in the testing of Generation 4 and 5 prototypes that temperature reduction is not assured even if the modified cell has a lower thermal resistivity than the standard cell due to low contact area.

The code simplifies the path the heat takes when reaching the copper by assuming the heat travels perpendicular to the solar cell inside the copper and then moves parallel to the solar cell through the copper, starting from the furthest edge of the copper inside the solar cell.

The code also considers that the length of the thermal pad and copper strip covering the side of the cell is 10 cm and the distance heat travels from the cell to the outside environment is 4 mm. Both parameters are design choices.

For a 0.3 mm thick copper strip, the optimal length of the inscription was determined to be around 1.69 cm.

The code is present in the Appendix.

3.7.2 Sensitivity Analysis of the conductivity of the Heat Pad

Variation of the thermal conductivity on the pad was done to study its effect on the cooling potential. The conductivity of the thermal pad varied between 1 and 200W/mK with a resolution of 1W/mK.

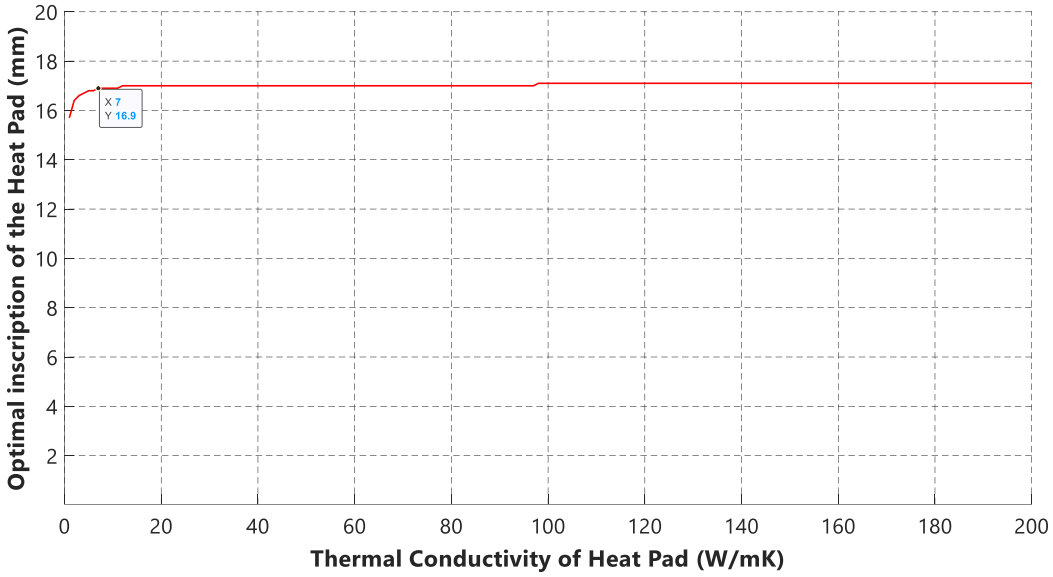

Figure 39- Sensitivity Analysis of the Optimal length of an inscription concerning the thermal conductivity of the Heat Pad

We can see that the optimal inscription length remains almost constant at 1.69 cm after the thermal conductivity reaches 7W/mK.

We can conclude that the conductivity of the thermal pad does not have a significant impact on the inscription length of the copper and thermal pad, as the limiting factor is the thermal resistivity in the path the heat has to follow while moving horizontally through the copper towards the outside environment having a high distance over area ratio.

3.8 Generation 6- Prototypes

To reduce the cooling effect of convection at the edges of the glass, a 2 x 2 configuration of solar cells was laminated on a 60 cm x 60 cm glass. A more extensive glass sheet increased the module's mass and reduced heat flow traveling across it. This change provided a better understanding of the temperature reduction and facilitated the installation of the manufactured modules at TU Delft facilities.

Decreasing the path that heat has to travel through the copper towards the surrounding was important. To this end, cuts were made to the EVA and the Tedlar. These were located around 4mm from the cells' edges to wedge the copper strips better.

(a) (b)

Figure 40- a) Setup for test procedure on May 8, 2022 b) Thermocouple connections for test on May 8, 2022

As seen in figure 40, the first model created used a white Tedlar with a copper of 0.3 mm thickness indented by around 1 cm and a length of 10 cm. The copper strips used were bent so that air would have a larger surface area to cover, aiding natural convection.

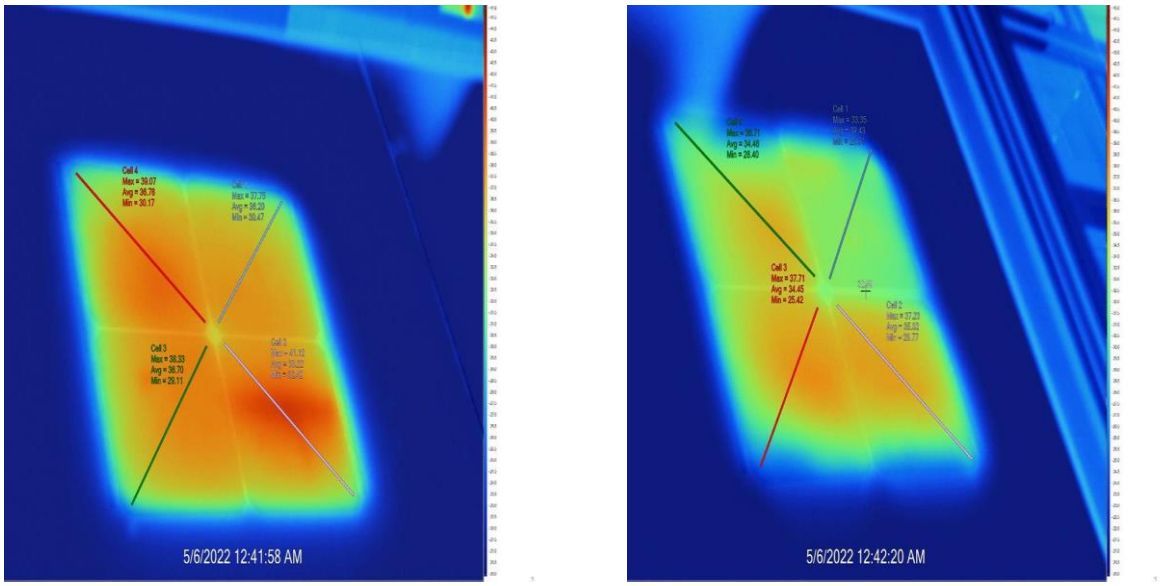

(a) (b)

Figure 41- a) Infrared image of Standard module b) Infrared image of the Test module.

In figure 41a, we can see that all the cells in the Standard module have a similar temperature profile. In figure 41b, we can see that the coolest areas are where the copper strips have been deployed, which causes the entire average temperature of the cells to decrease compared to the Standard cell.

3.8.1 Test 1

Test condition: Outdoor testing

Test Duration: 6 days

All thermocouples were placed in the center of the cells

Present in the graph is the most representative day to make sure the data is comprehensible

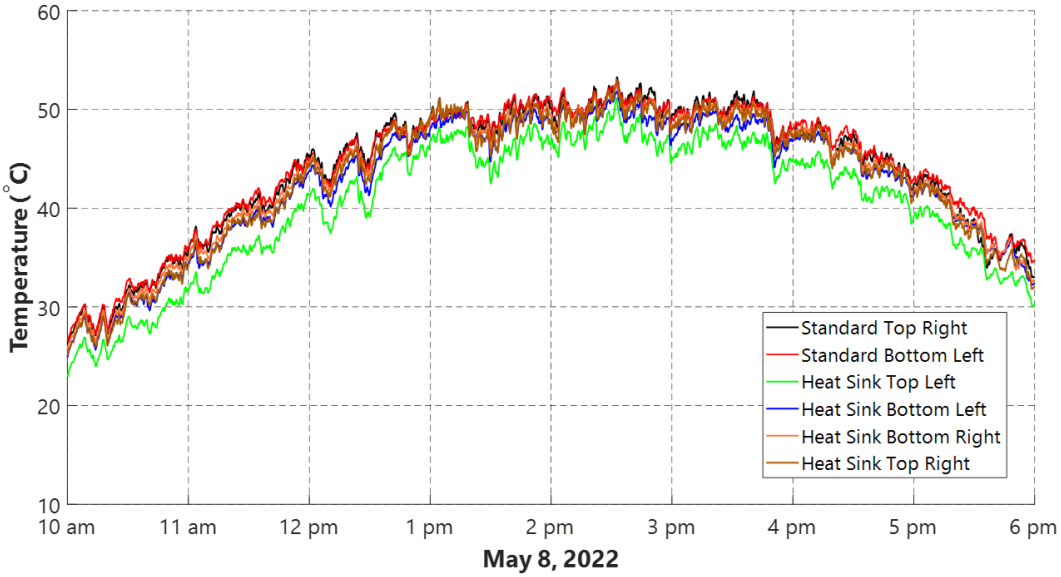

Figure 42- Outdoor testing of Test module May 8, 2022

Table 13- Maximum temperature reduction achieved with regards to the Standard module

Thermocouple Position	Temperature reduction compared to the average of the Standard cells.
Heat sink Top Left cell	Max of 5.49°C
Heat sink Bottom Left	Max of 2.98°C
Heat sink Bottom Right	Max of 2.26°C
Heat sink cell Top Right	Max of 2.44°C

Observations

The maximum temperature reduction was observed at the cell located in the Top Left position of the 2x2 module, around 7-8°C. For the same design, cell number 1 was performing significantly better. The backside Tedlar was cut open to see what length of copper was indented into the cell to emulate the result on the following prototypes.

When the cut was performed, it was evident that the copper had surpassed the thermal pad limit and made contact with the cell, which caused lower temperature readings and the copper strip to be at a higher temperature.

It was not expected that the copper strips would have touched the solar cell because measurements were performed under the solar simulator, where the output of Generation

6 Prototype was Isc=0.64 A and Voc= 2.25 V, whereas the output of the Standard module was Isc=0.64 A and Voc= 2.35 V, not suggesting any short circuit in the cells.

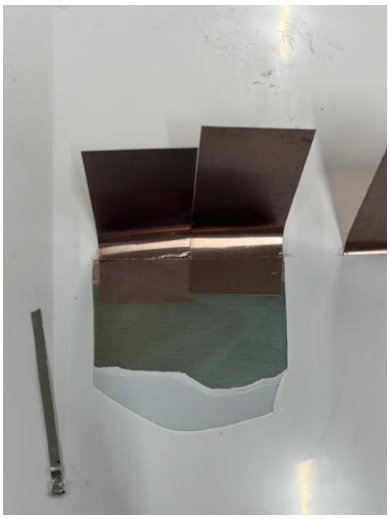

Figure 43- Defective attachment of the copper strip

Although the prototype was defective, it did suggest that extending the copper further in the cell would increase heat extraction.

3.9 Generation 7- Prototypes

Transparent Tedlar was used to alleviate the uncertainty associated with placing the copper strips on the thermal pad due to the opaqueness of white Tedlar.

The Matlab code calculated that the maximum heat would be extracted from the cell if the copper strips were indented around 1.69 cm.

The first model, seen in figure 44, used a transparent Tedlar with a copper of 0.3 mm thickness indented by around 1.75 cm and a length of 10 cm across the side of the cell.

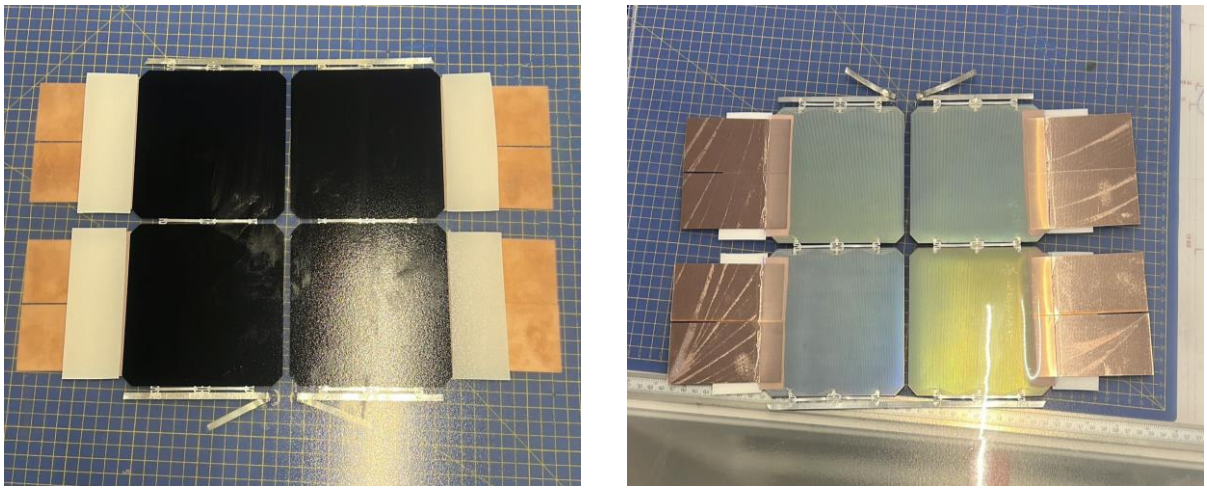

(a) (b)

Figure 44- a) Frontside view of Concept (1.75cm/0.3mm) b) Backside view of Concept (1.75cm/0.3mm)

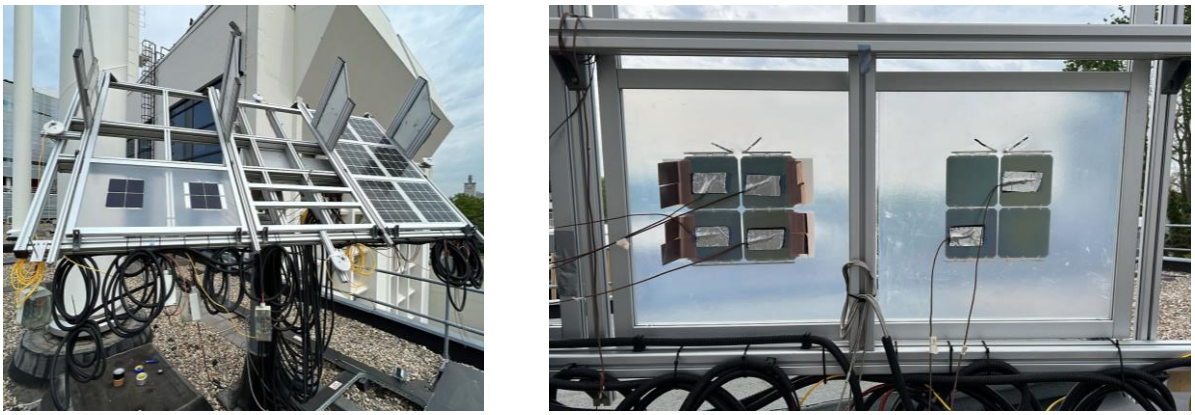

(a) (b)

Figure 45- a) Setup for test procedure on May 11, 2022, b) Thermocouple connections on May 11, 2022

3.9.1 Test 1

Test condition: Outdoor testing

Test Duration: 3 days

All thermocouples were placed in the center of the cells

Present in the graph is the most representative day to make sure the data is comprehensible.

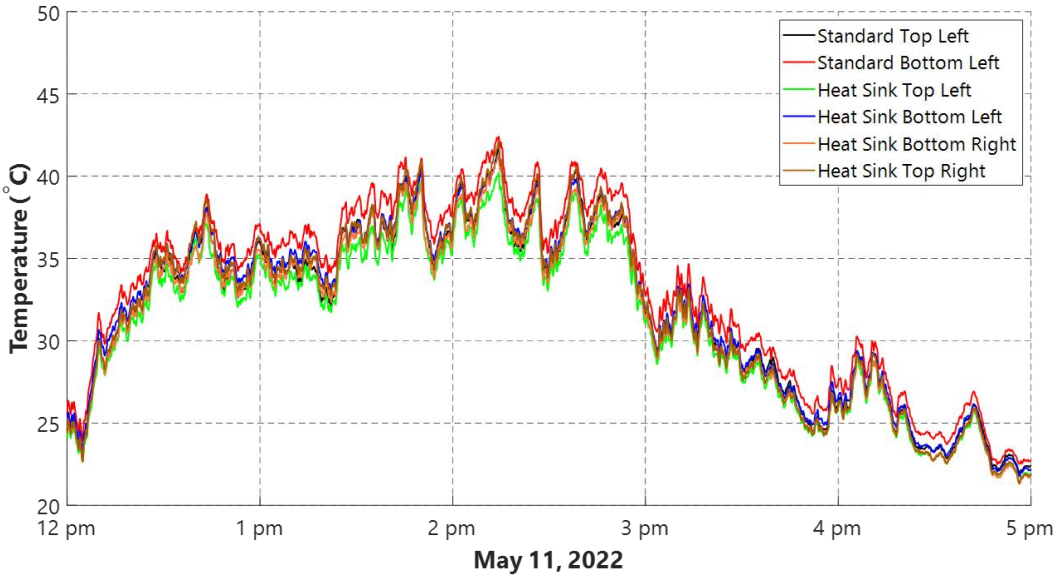

Figure 46- Outdoor testing of Concept(1.75cm/0.3mm) May 11, 2022

Observations

The cell in the Top Left position of the Heat Sink performed the best as it recorded the lowest temperature compared to the Standard cells. A temperature reduction between 1-3°C was observed.

Table 14- Maximum temperature reduction achieved with regards to Standard module

Thermocouple position	Temperature reduction compared to the average of the Standard cells.
Heat sink Top Left	Max of 2.57°C
Heat sink Bottom Left	Max of 1.35°C
Heat sink Bottom Right	Max of 2.07°C
Heat sink Top Right	Max of 1.44°C

3.10 Generation 8- Prototypes

A module was created to test the effect of the length of inscription of the copper strip on heat extraction. The module will also validate the Matlab model. For this device, the selected lengths of inscription for the thermal pad and the copper strip were 0.8 cm. The copper strips had a thickness of 0.3 mm and a length of 10 cm.

A module was created with a copper thickness of 0.5 mm to test the effect of the thickness of the copper strip on heat extraction. This module had a length of inscription of 1 cm for the thermal pad and the copper strip. The length of the copper strip was 10cm.

Figure 47- Setup for test procedure on May 15, 2022

3.10.1 Test 1

Test condition: Outdoor testing

Test Duration: 5 days

All thermocouples were placed at the center of the cells. The best-performing cell from each model is presented in figure 48.

Present in the graph is the most representative day to make sure the data is comprehensible.

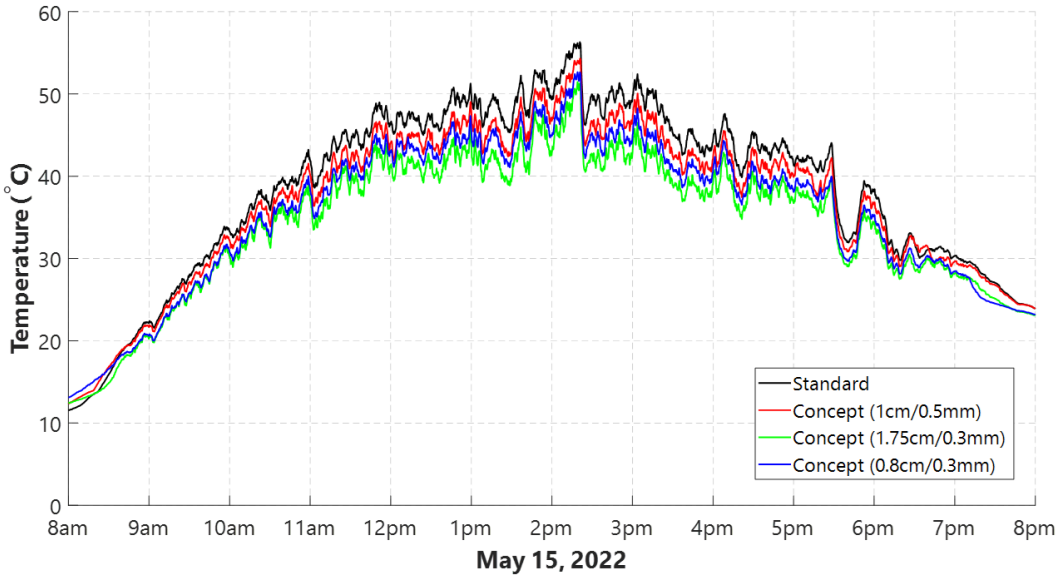

Figure 48- Outdoor testing of Concept(1.75 cm/0.3 mm), Concept(1 cm/0.5 mm) and Concept(0.8 cm/0.3 mm) May 15, 2022

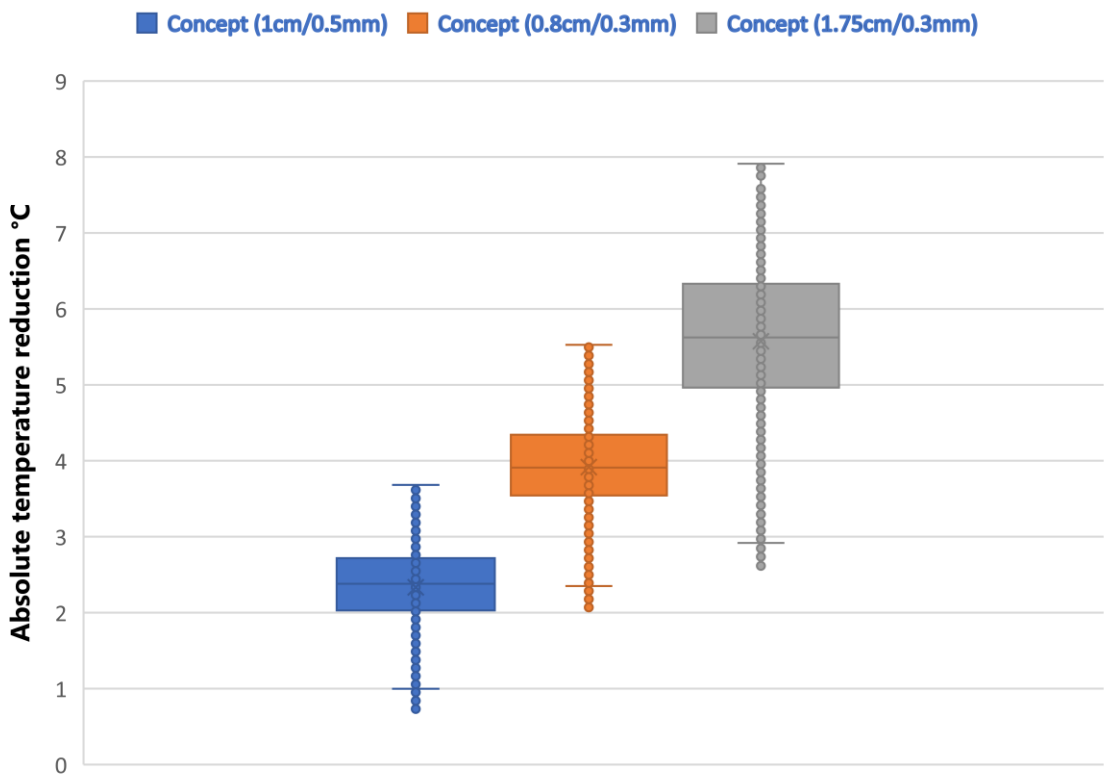

Figure 49- Absolute temperature reduction for the concepts tested on May 15, 2022, from 10:30 am to 6 pm

The models were specified according to the copper strip's inscription length and thickness. Hence Concept (1.75cm/0.3mm) refers to the model with a 1.75 cm length of inscription and 0.3 mm thickness of the copper.

3.10.2 Observations

Concept (1.75 cm/0.3 mm) having an indentation of around 1.75cm with a copper thickness of 0.3 mm performed best. Comparing the Concept (1 cm/0.5 mm) having an indentation of around 1cm with a copper thickness of 0.5mm to the Concept (0.8 cm/0.3 mm) having an indentation of around 0.8 cm with a copper thickness of 0.3 mm, we see that Concept (0.8cm/0.3mm) outperforms Concept (1 cm/0.5 mm) in heat extraction capacity even though Concept (1 cm/0.5 mm) had a higher indentation of the copper used. Therefore, the thinner the copper used, the higher the heat extraction capability.

3.11 Generation 9- Prototypes

Two additional modules were produced to validate the one-dimensional Matlab model that calculated the optimal length of indentation of the copper strip. The first one had a length of inscription of 2.35cm for the thermal pad and the copper strip. The copper strips had a thickness of 0.3 mm and a length of 10 cm. The second one had a length of inscription of 4 cm, longer than the optimal length for the thermal pad and the copper strip. The strips had a thickness and a length of 0.3 mm and 10 cm on each cell's side, respectively.

Figure 50- Setup for test procedure on May 22, 2022

3.11.1 Test 1

Test condition: Outdoor testing

Test Duration: 13 days

All thermocouples were placed at the center of the cells. The best-performing cell from each model is shown in figure 51.

Present in the graph is the most representative day to make sure the data is comprehensible.

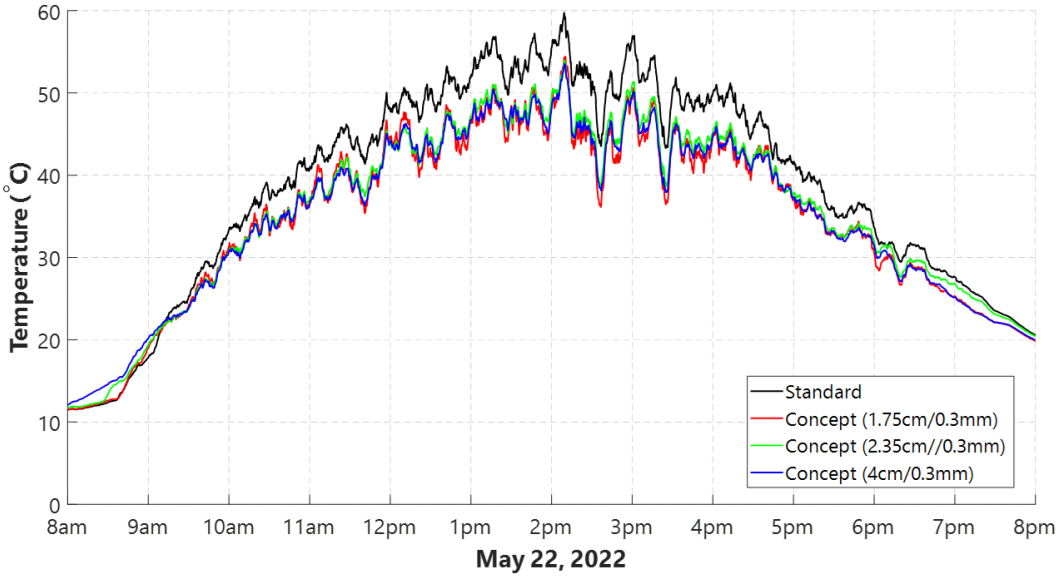

Figure 51- Outdoor testing of Concept(1.75 cm/0.3 mm), Concept(2.35 cm/0.3 mm) and Concept(4 cm/0.3 mm) May 22, 2022

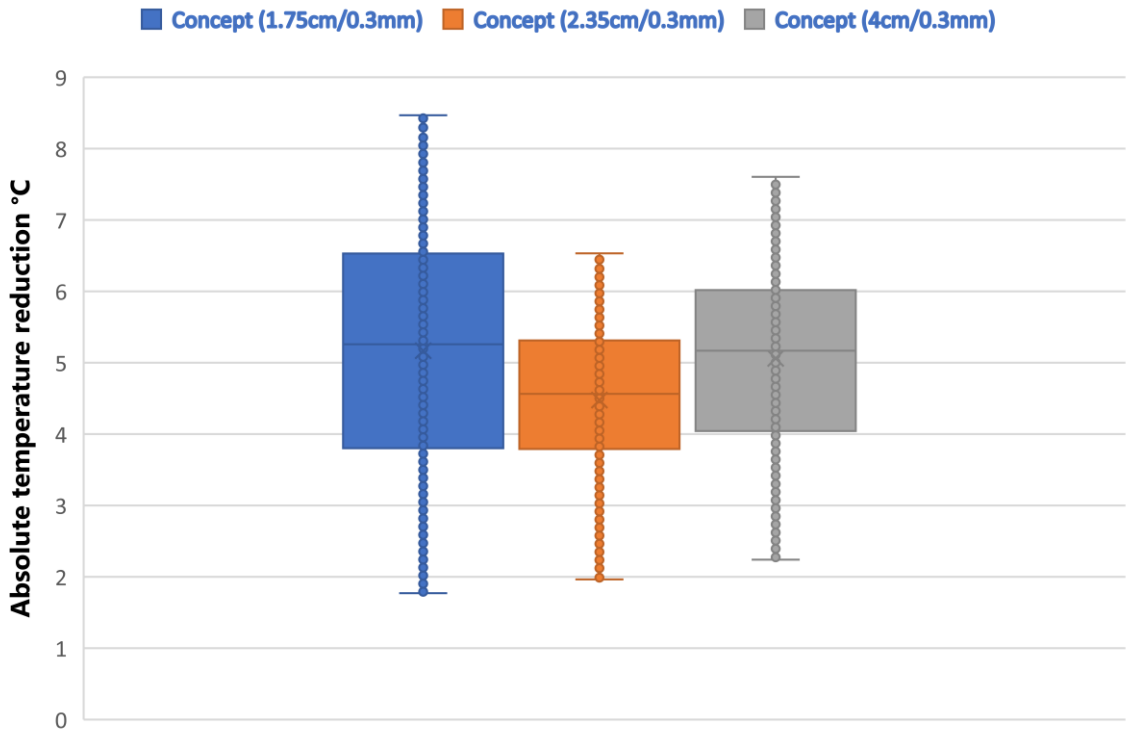

Figure 52- Absolute temperature reduction for the concepts tested on May 22, 2022, from 10:30 am to 6 pm

Observations

From the measurements, we can conclude that having the copper strips inscribed at around 1.75 cm achieves the most significant temperature reduction. The copper strips

inscribed at any distance lower than 1.75 cm reduce the temperature reduction capabilities. However, having copper inscribed further into the cell, the cell does not perform much worse, as the difference in temperature reduction was less than 1°C, so it can be said that after 1.75 cm of inscription, the temperature reduction achieves saturation.

3.11.2 Remarks

At a relatively constant level of irradiance, the module having copper strips inscribed 1.75 cm into the cell performs best. With a sharp increase in the level of irradiance, as in the case of a clear sky right after a long period of cloudy sky, the module having the largest inscription of copper into the cells performs best as the presence of more copper inside the cell allows for more direct storage of heat inside the copper reducing the temperature of the cell faster. A more extended period of exposure to constant irradiance sees this trend correct itself to the initial best-case scenario.

The opposite is also true, as temperature reduction in the cell with the lowest amount of copper directly behind the cell sees its temperature reduce the quickest when the sun disappears as cooling of the copper part behind the cell is faster.

The higher the level of irradiance and temperature in the surrounding environment, the more temperature reduction is observed.

The thinner the copper strip, the higher the heat extraction potential for the same inscription length.

3.12 Effect of Irradiance and Cell Temperature on Temperature Reduction Concept (1.75cm/0.3mm)

The temperature reduction achieved by the Concept (1.75 cm/0.3 mm) is calculated by taking the difference between the average temperature of the thermocouple sensors on the Concept (1.75 cm/0.3 mm) and the ones on the Standard module.

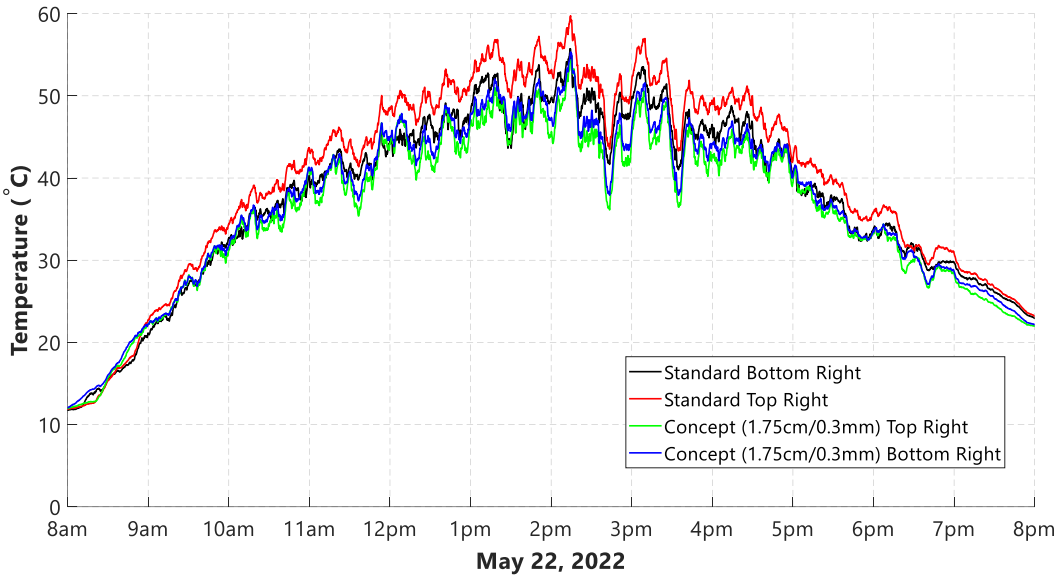

Figure 53- Outdoor testing of Concept (1.75 cm/0.3 mm) on May 22, 2022

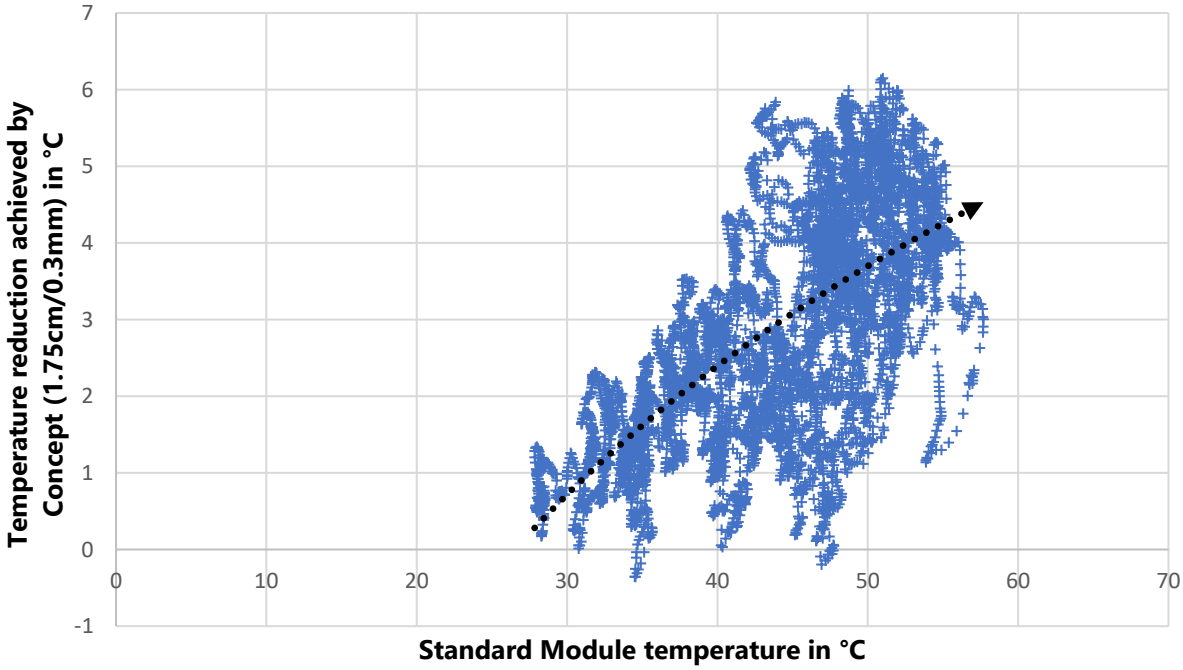

Figure 54- Temperature reduction achieved by Concept (1.75 cm/0.3 mm) on May 22, 2022

In figures 53 and 54, we can see that as the temperature of the Standard module increases due to surrounding environmental temperature and irradiance, the temperature reduction achieved by the Concept (1.75 cm/0.3 mm) increases. Hence more heat is extracted when the solar cell is exposed to more irradiance. The maximum temperature reduction achieved by the Concept (1.75 cm/0.3 mm) on May 22, 2022, was around 6.16°C.

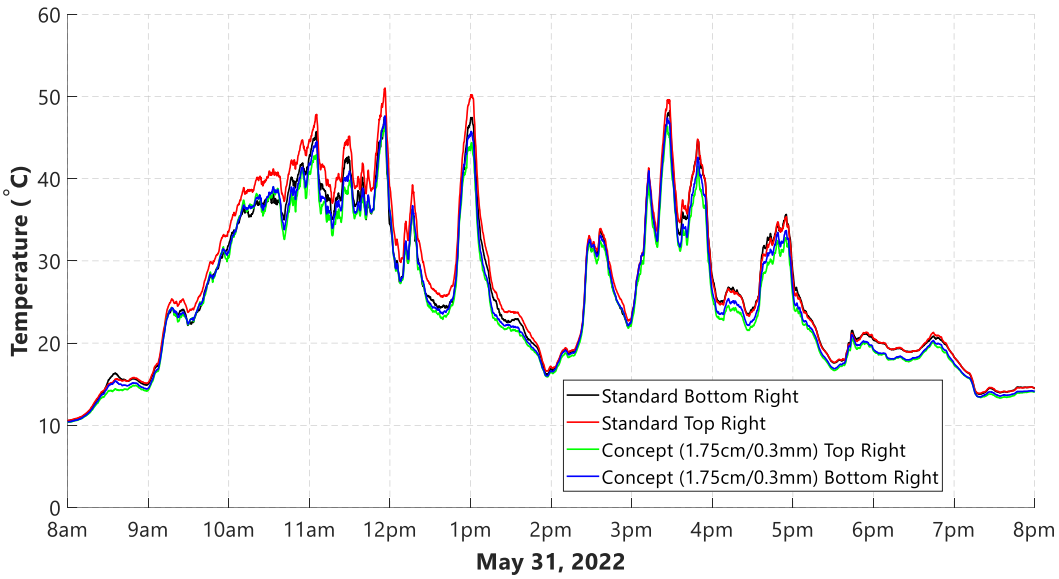

Figure 55- Outdoor testing of Concept (1.75 cm/0.3 mm) on May 31, 2022

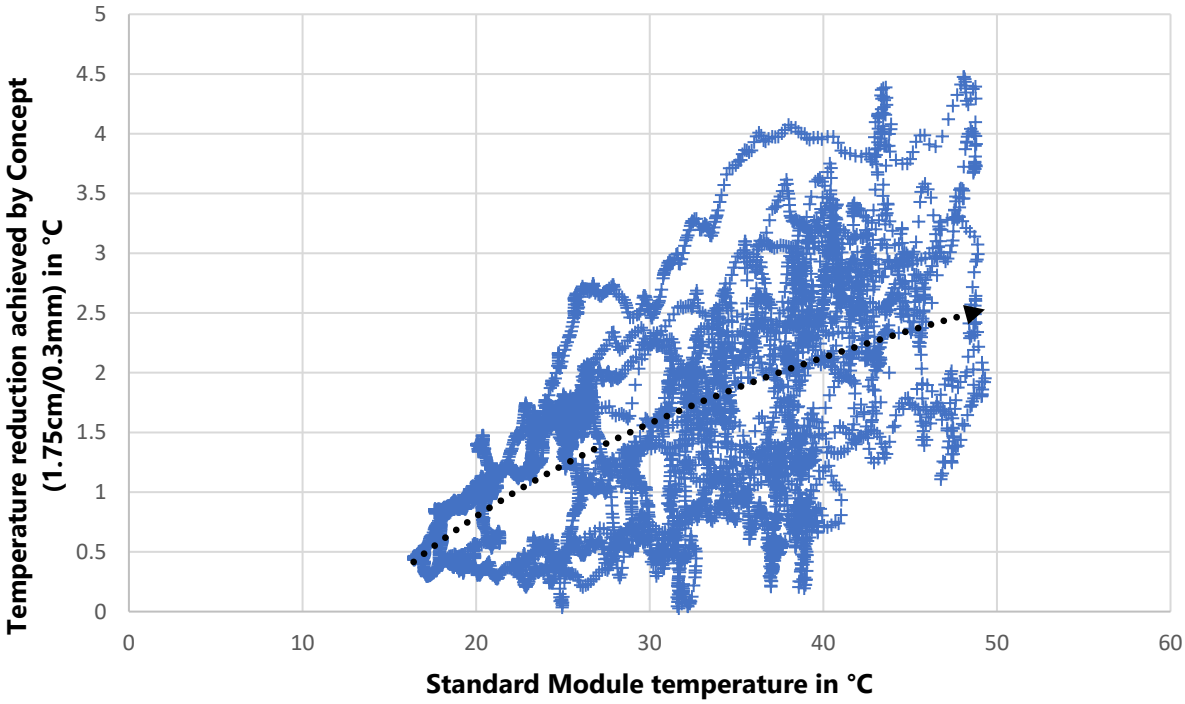

Figure 56- Temperature reduction achieved by Concept (1.75cm/0.3mm) on May 31, 2022.

In figures 55 and 56, we can also see that as the temperature of the Standard module increases due to surrounding environmental temperature and irradiance, the temperature reduction achieved by the Concept (1.75 cm/0.3 mm) increases. Hence more heat is extracted when the solar cell is exposed to more heat. The maximum temperature reduction achieved by the Concept (1.75 cm/0.3 mm) on May 31, 2022, was around 4.52°C.

Comparing the results on May 22 and May 31 shows that at the same Standard Module temperatures, the temperature reduction achieved on May 22 is higher than the temperature reduction achieved on May 31. These lower values could be due to discontinuous irradiance levels, leading to large fluctuations in the measured temperature of the cells. The fact that copper is used in the modified modules leads to a delay in the cooling and heating of each cell because of copper's volume and heat capacity. Hence sudden fluctuations reduce the temperature extraction potential of the Concept (1.75 cm/0.3 mm) compared to a day with continuous levels of irradiance similar to May 22 because of heat stored inside the copper strip.

3.13 Generation 10- Prototypes

After identifying the optimal inscription length for the copper strips on the edges, a 3x3 configuration of solar cells was used in a 60cmx60cm glass to figure out an optimal way to extract heat from the central cells.

Design 1 and Design 2 were considered while trying to implement the internal heat sinks on a 3x3 module.

The concept behind Design 1 was to create a thermally connected circuit between each horizontal row in the 3x3 matrix, where heat would travel from the central cell to the ones on the edges, where they would then be extracted.

Whereas Design 2 focused on extracting the heat from each cell itself. The middle cells had an internal heat sink placed in the center since the central part of the cell is heated the most. In Design 2, the indentation of copper in the middle cell had a width of around 4.6 cm. Since the copper is extracted directly from inside the cell, no offset is needed, and it has an outlet on both sides of the copper strip. Hence the optimal distance of inscriptions is (1.69cm*2 + 0.4cm*2) = 4.18cm.

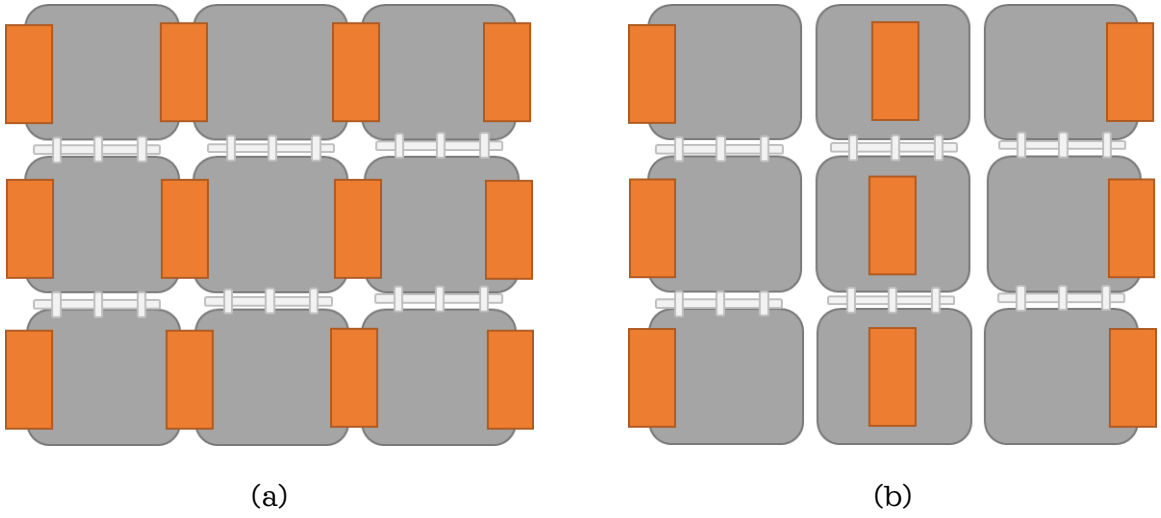

Figure 57-a) Backside view of concept Design 1 b) Backside view of concept Design 2

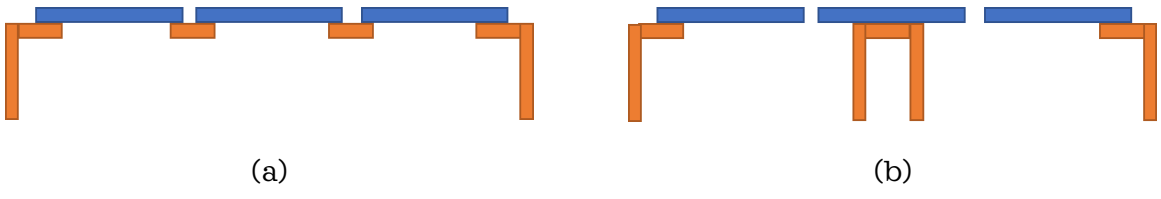

Figure 58- a) Side view of concept Design 1 b) Side view of concept Design 2

Table 15- Design specifications for Module Design 1 and Design 2

	Thermal Pad		Copper plate	
Module Design	**Thickness (mm)**	**Surface Area (mm^2)**	**Thickness (mm)**	**Surface Area (mm^2)**
Design 1	0.5	48*50	0.3	46*50
Design 2	0.5	48*50	0.3	46*50

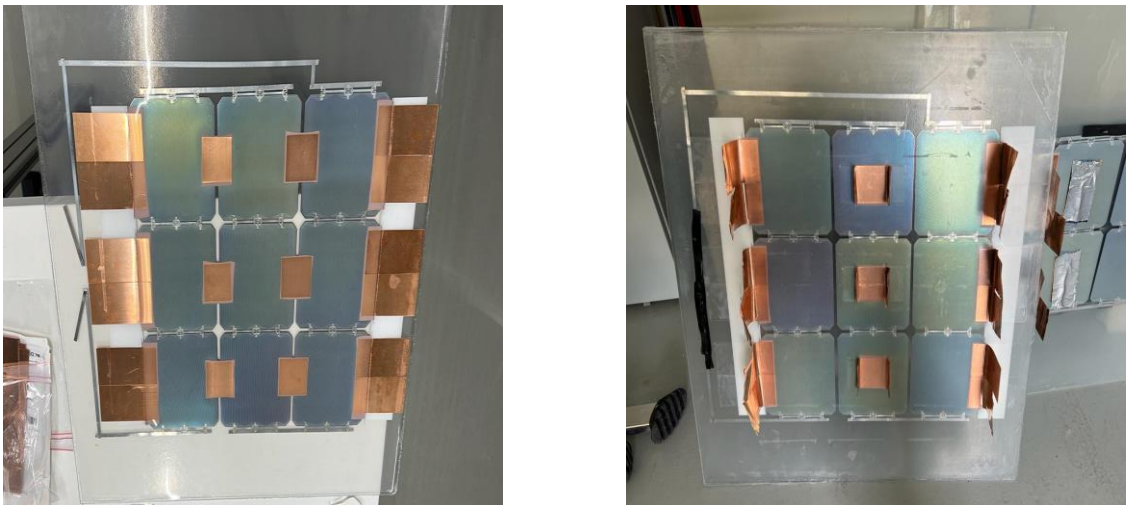

(a) (b)

Figure 59- a) Backside view of manufactured Design 1 b) Backside view of manufactured Design 2

Electroluminescence (EL) was also carried out on both designs. It was found that the module with Design 1 had a minor crack in the top left corner, whereas Design 2 had no cracks.

Current and Voltage measurements were performed on both designs, and no issue was evident on the energy production side.

All measurements done on Design 1 were far away from the damaged cell.

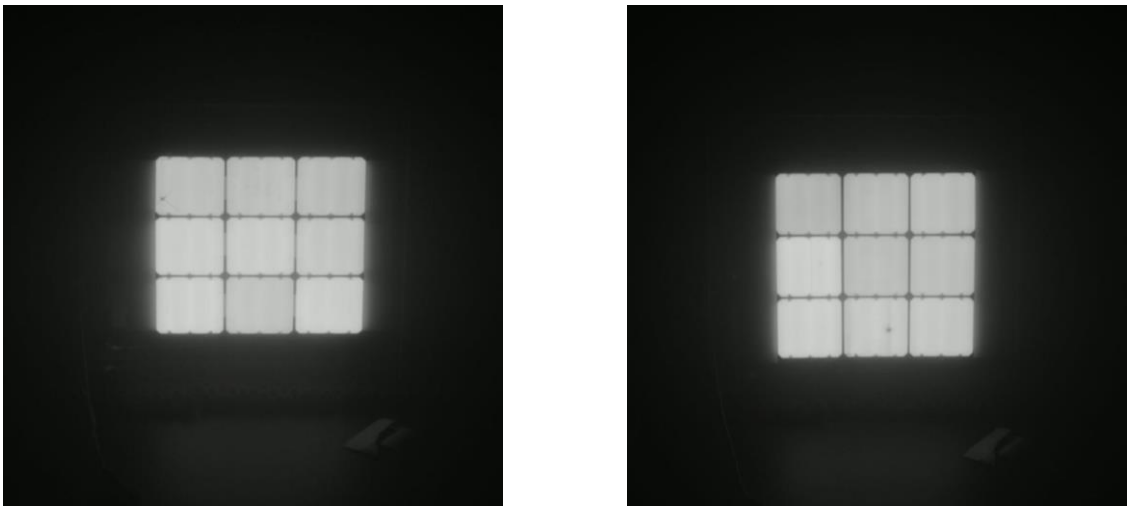

(a) (b)

Figure 60- a) Electroluminescence (EL) test on Design 1 b) Electroluminescence (EL) test on Design 2

Figure 61- Setup for test procedure on June 3, 2022

3.13.1 Test 1

Test condition: Outdoor testing

Test Duration: 13 days

All thermocouples were placed at the center of the cells. The best-performing cell from each model is shown in figure 62.

Present in the graph is the most representative day to make sure the data is comprehensible.

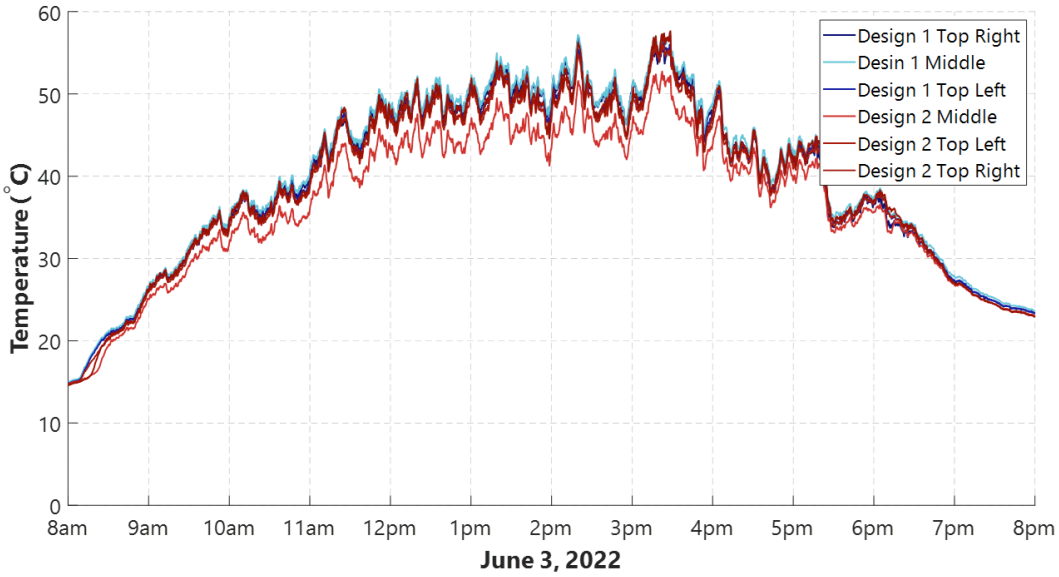

Figure 62- Outdoor testing of Design 1 and Design 2 June 2, 2022

Observations

It can be seen that Design 2 performed marginally better than Design 1, as almost all the tested cells in Design 2 had lower temperatures recorded than the cells in Design 1 throughout the entire day.

3.14 Integrating Frames

The idea of attaching the protruding copper strips to a frame was studied in order to increase the cooling potential of the internal heat sinks. Different designs of frames were thought of, all with the idea of sandwiching or being able to attach the copper strip to the aluminum frame.

Design 1, seen in figure 63, uses other aluminum bars that need to be added to sandwich the copper strips protruding out of the PV module. The additional aluminum bars need to be attached mechanically to the original frame of a PV module.

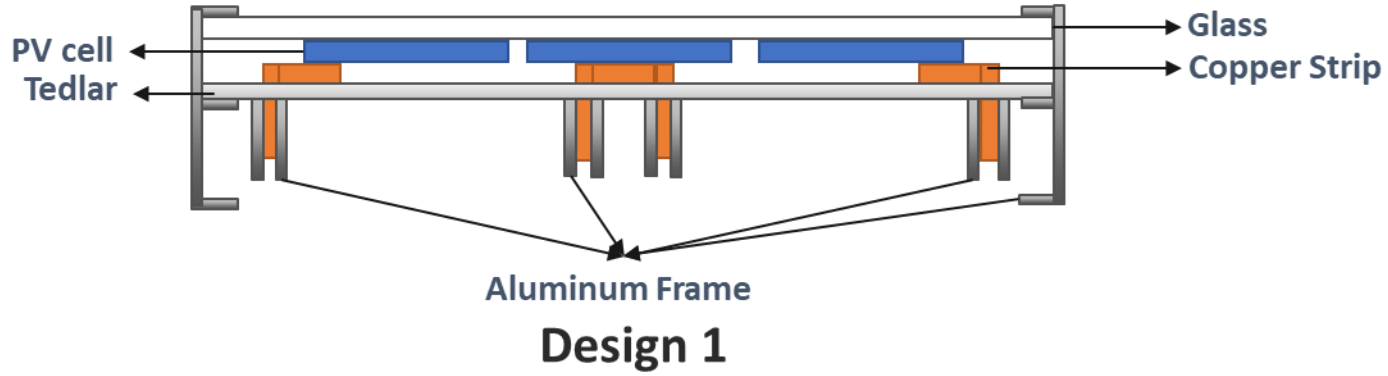

Figure 63- Frame design concept 1 for PV module

Design 2, which can be seen in figure 64, uses a slightly modified PV module frame. Additional aluminum bars are fixed at the edges of the frames to sandwich the copper strips protruding from the PV module. The additional aluminum bars can be welded to the original frame of a PV module. Design 2 for the frames is a simpler model as it allows for more airflow in the center of the PV module, increasing natural convection.

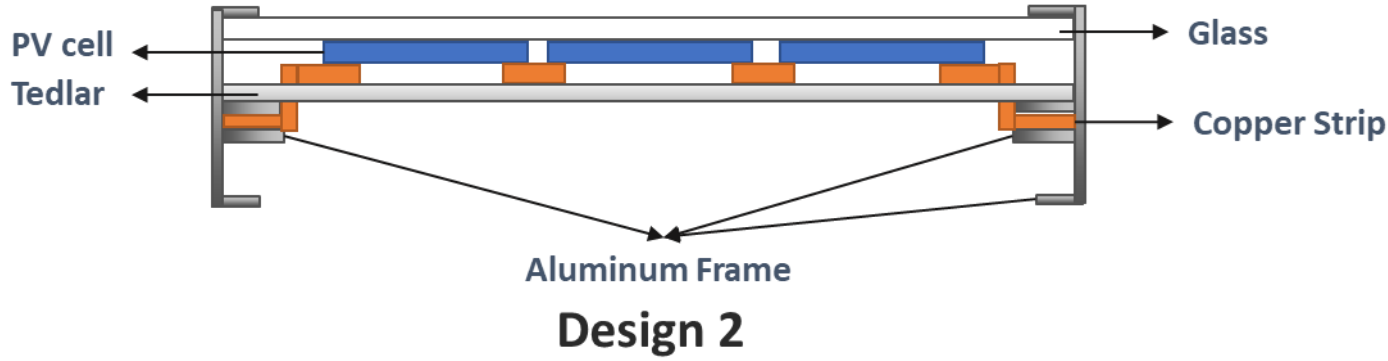

Figure 64- Frame design concept 2 for PV module

Although Design 2 for the frames is more straightforward in comparison, Design 1 was chosen as the final frame design, which was used in testing as it allows for the complete coverage of all the copper strips, which would have been an issue with Design 1.

Hence, custom frames were ordered and delivered having frame Design 1 in mind. The Standard 3x3 module and Design 2 module were put in the customized frames to simulate similar test conditions. Design 2 module was chosen over Design 1 module for the final test as it had better performance in the previous temperature test.

(a) (b)

Figure 65- a) Setup for test procedure on June 10, 2022 b) Thermocouple connections for test on June 10, 2022

3.14.1 Test 2

Test condition: Outdoor testing

Test Duration: Started June 10, 2022

All thermocouples were placed at the center of the cells. The average temperature of the thermocouples on each module is shown in figure 66.

Present in the graph is the most representative day to make sure the data is comprehensible.

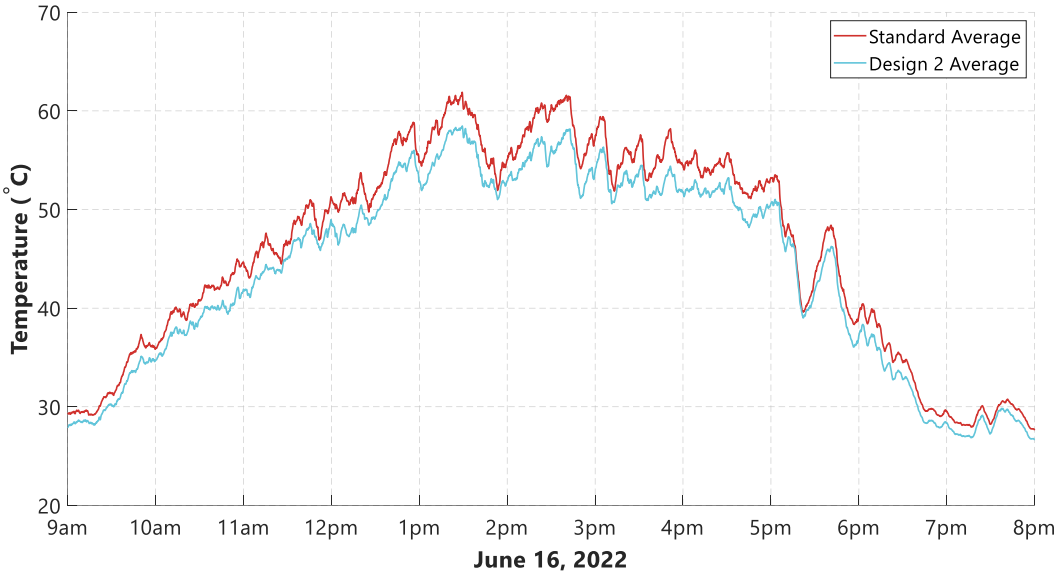

Figure 66- Outdoor Testing of Design 2 on June 16 (1)

Observations

When we averaged out the temperature of the sensors attached to Design 2 and compared them to the average temperature of the Standard module, Design 2 presented a lower temperature throughout the entire June 16. The maximum temperature reduction achieved was 4.75°C. It is important to note that a sudden decrease in the level of irradiance was observed at a quarter to 2 pm, leading to a decrease in the temperature of the Standard module and Design 2. The Standard module saw a relatively faster decrease in temperature as the absence of copper makes the cooling of the PV cell much quicker due to the high heat capacity of the copper.

3.15 Effect of Irradiance and Cell Temperature on Temperature Reduction Design 2

The temperature reduction achieved by Design 2 is calculated by taking the difference between the average temperature of the thermocouple sensors on Design 2 and the ones on the Standard module.

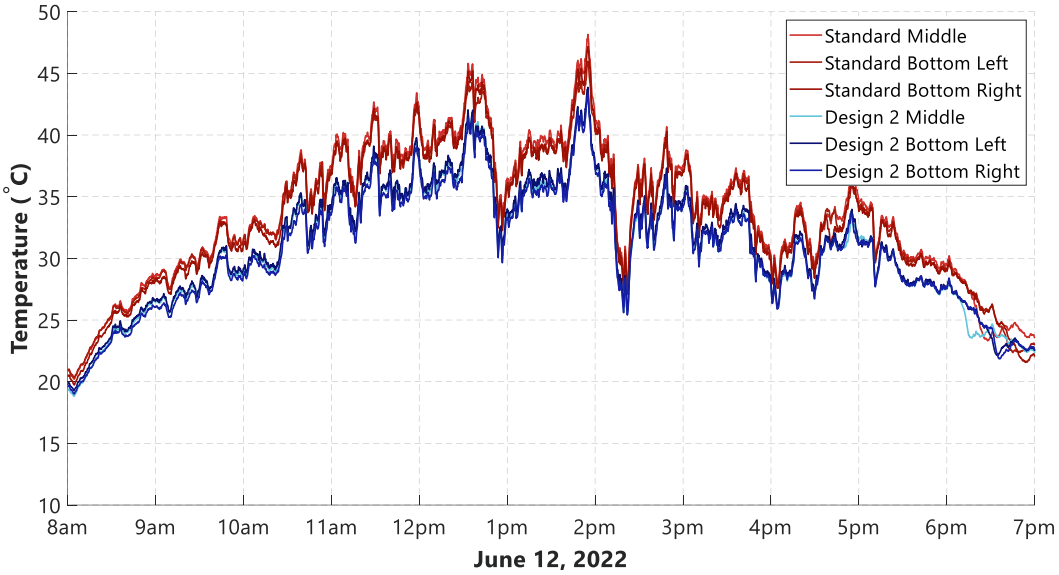

Figure 67- Outdoor Testing of Design 2 on June 12, 2022

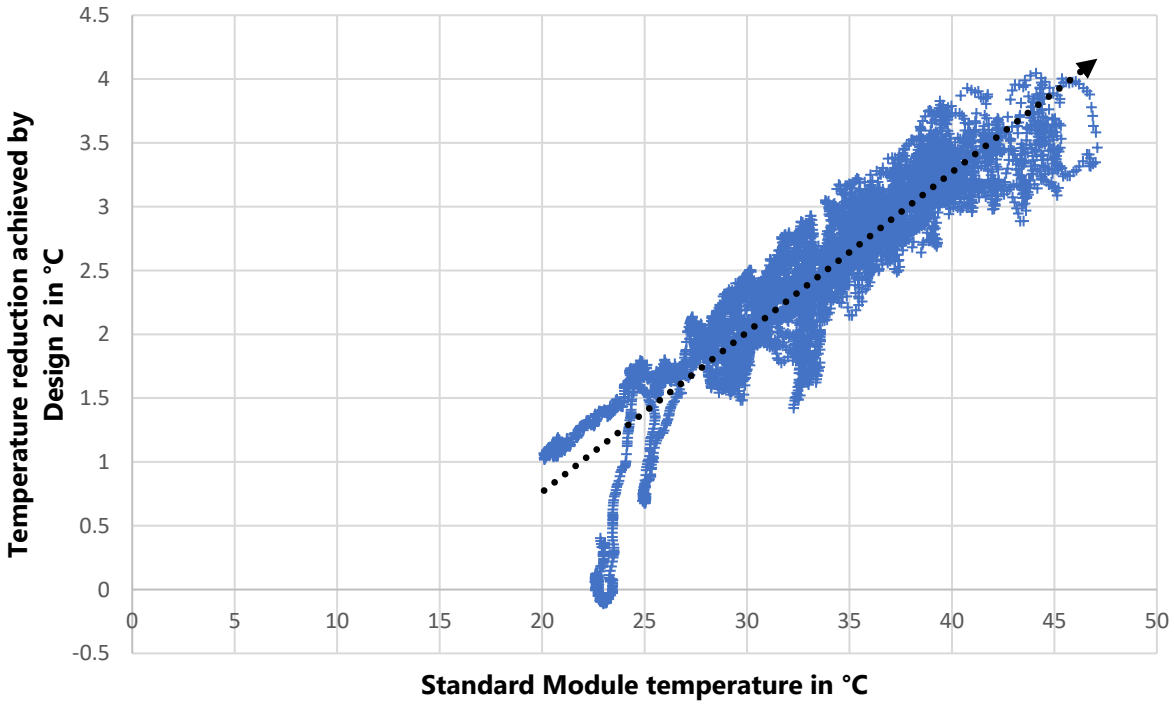

Figure 68- Temperature reduction achieved by Design 2 on June 12, 2022

The maximum average temperature reduction achieved on the June 12 was around 4.05°C. Conditions on June 12 are considered as moderate levels of irradiance with moderate levels of disturbances characterized by significant temperature variations in a short timeframe.

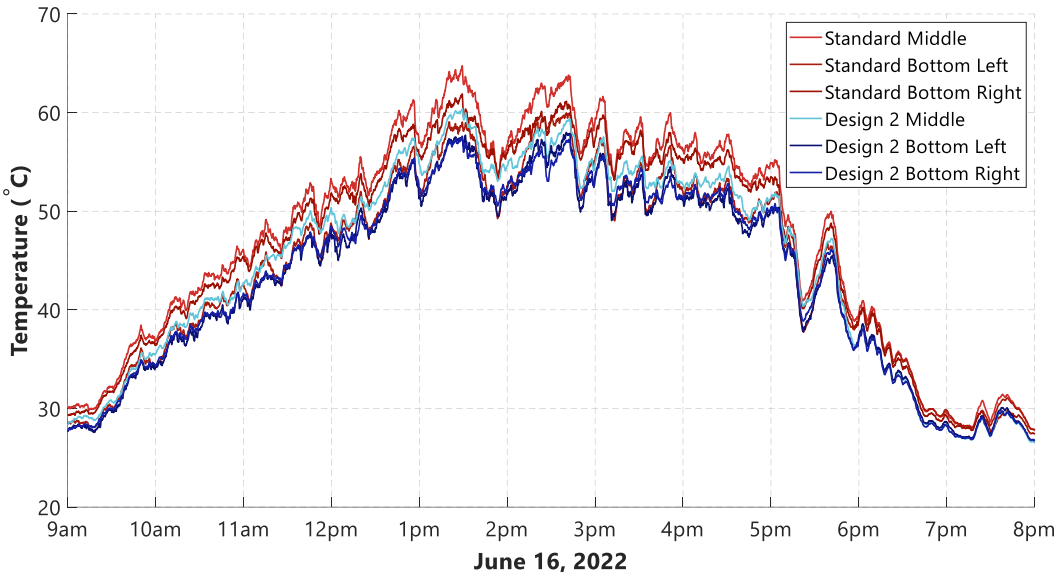

Figure 69- Outdoor testing of Design 2 on June 16, 2022 (2)

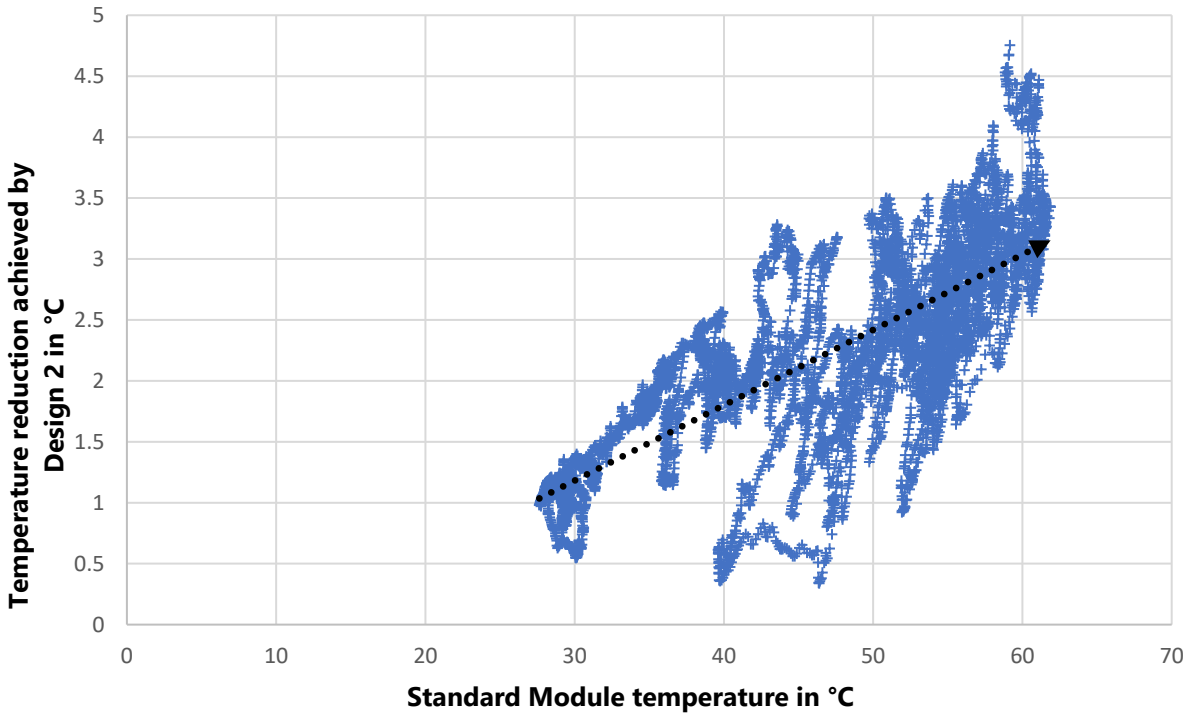

Figure 70- Temperature reduction achieved by Design 2 on June 16, 2022.

The maximum average temperature reduction achieved on June 16 was around 4.75°C. Conditions on June 16 are considered high levels of irradiance with moderate levels of disturbances characterized by large levels of temperature variations in a short timeframe.

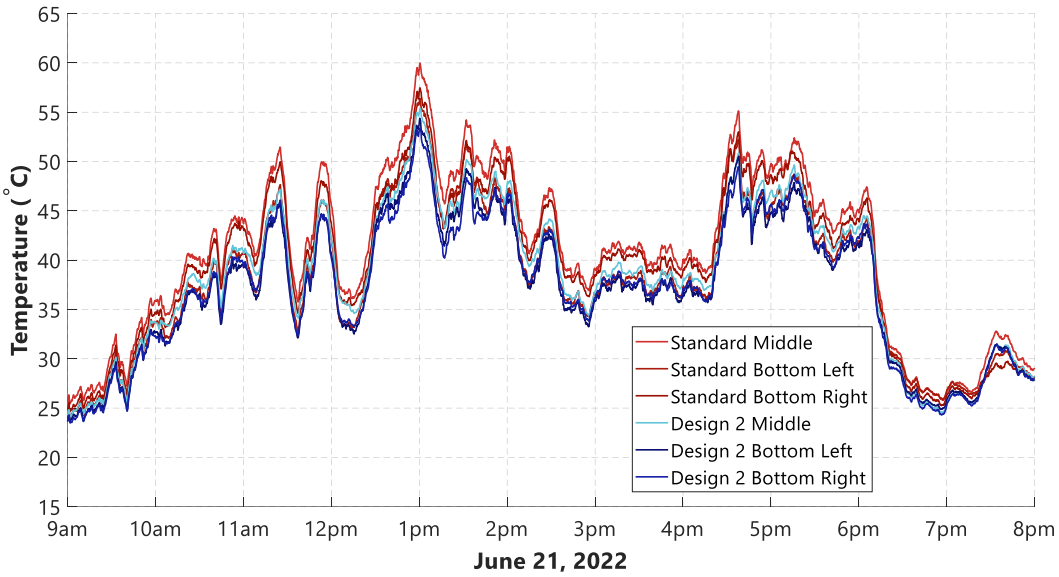

Figure 71- Outdoor testing of Design 2 on June 21, 2022

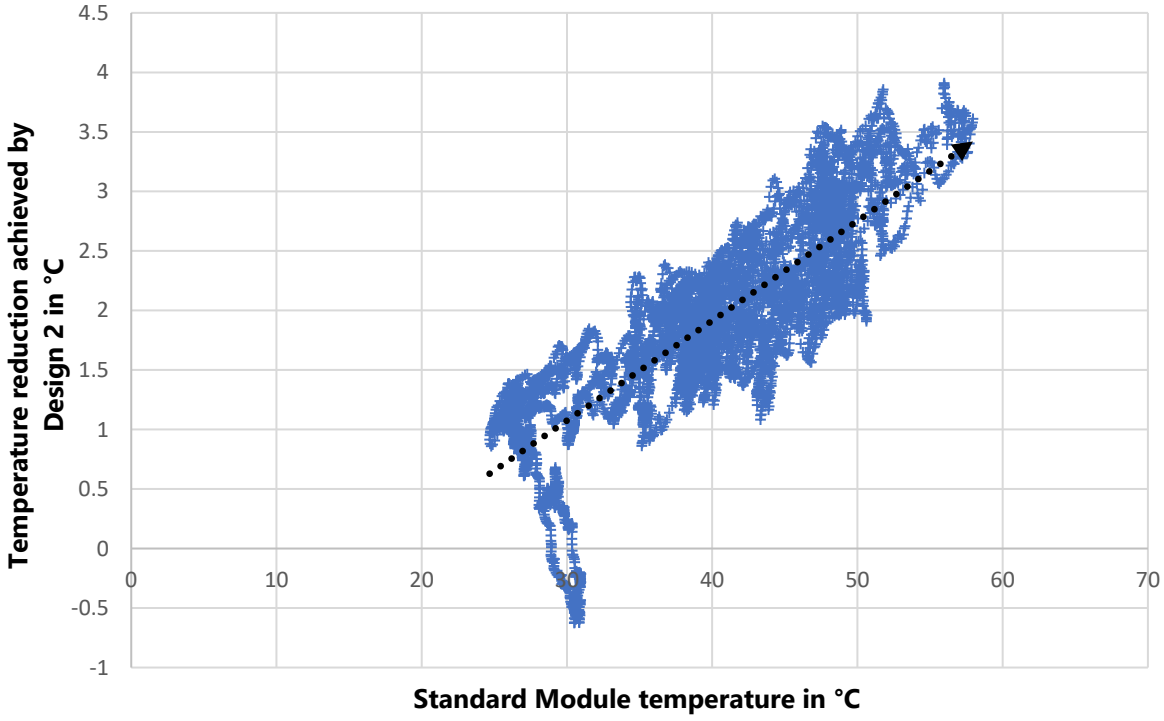

Figure 72- Temperature reduction achieved by Design 2 on June 21, 2022

The maximum average temperature reduction achieved on June 21 was around 3.91°C. Conditions on June 21 can be considered as moderate levels of irradiance with high levels of disturbances characterized by large temperature variations in a short timeframe.

From the above graphs, we can observe that, as seen in the tests done on the Concept (1.75 cm/0.3 mm), the same applies to Design 2. A higher Standard module temperature due to an increase in irradiance leads to a higher temperature reduction potential.

Moreover, as can be seen in tests done on the Concept (1.75 cm/0.3 mm), disturbances in levels of irradiance mainly characterized by the appearance of clouds significantly affect the temperature reduction potential of Design 2 as well. This disturbance is apparent since the temperature reduction achieved on June 21 has the highest fluctuations, the lowest between the three represented days, even though there are times throughout the day when the Standard module temperature exceeds 50°C.

It can also be seen that the maximum temperature reduction was achieved on June 16 with a temperature reduction of 4.75°C. Almost similar disturbances characterized by a sudden increase or decrease in temperature of the cells can be observed on June 12 and 16. This behavior means that the sun was present the same way on both days. Moreover, we can see that the temperature of the Standard module on June 16 reached a higher level, meaning that the power of the incident rays was higher, leading to more heating of both cells and ultimately to more temperature reduction in Design 2. These results reaffirm the statement that an increase in solar irradiance leads to higher temperature reduction potential.

A combination of different environmental conditions leads to a large variety of temperature reduction ranges, meaning that it might be complicated to pinpoint at which conditions the optimal temperature extraction lies. With the gathered data, it can be expected that a day with high-level irradiance combined with low levels of cloud disturbances might lead to the highest potential for temperature reduction.

Table 16- Temperature reduction observed on different days for module Design 2

	June 12, 2022	**June 16, 2022**	**June 21, 2022**
Maximum Average Temperature Reduction	4.05°C	4.75°C	3.91°C
Maximum Temperature reduction of Middle cell	4.83°C	5.45°C	4.81°C
Maximum Temperature reduction of Bottom Left cell	3.63°C	3.89°C	3.02°C
Maximum Temperature reduction of Bottom Right cell	4.36°C	5.21°C	4.61°C

Table 16 shows the temperature reduction achieved on different days during the temperature recording by the thermocouples. It can be seen not only that the temperature reduction is different for each day but also that the temperature reduction is different for each cell. This trend is probably due to the modules' position, combined with the different heat profiles of the modules and wind profiles.

It can also be seen that on all the days, the temperature reduction achieved in the middle cell had the highest temperature value. This value could be that the cell in the middle of the module experienced the highest heating. Hence the highest temperature reduction was possible. However, it could also be that extracting heat by fixing the copper in the middle of the cell extracts more heat. It seems logical that the temperature reduction increases since the heat extracted come from the center of the cell, which reaches the highest temperature compared to other parts.

4 Cost Analysis

As the literature section showed, there is much research into different cooling techniques for both active and passive PV modules. Due to the need for a continuous energy supply, a simple cost analysis for active cooling methods is more complicated, and it is out of the scope of this work.

Focusing on the cost of implementing passive cooling techniques onto PV modules, at the time of this work, there was not any large-scale commercial passive cooling being implemented in the market to compare our technology.

An example of a passive cooling technology that almost made it onto the market is the "COOLBACK". "COOLBACK" is an innovation that replaces the conventional PV module frame and back sheet with a collection of fins, creating a form of a heat sink capable of increasing the energy output by around 7% (Coolback, 2021). However, the product never made it to the market as the company went bankrupt due to costs involved in manufacturing the product, such as the increase in the price of aluminum (Solar Magazine, 2021).

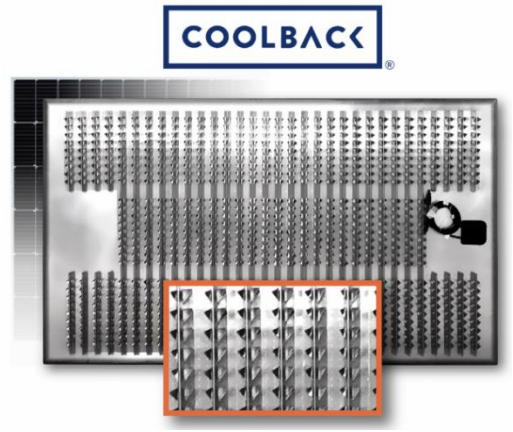

Figure 73- COOLBACK model (Coolback, 2021)

If we were to compare the costs involved by looking at the amount of material involved in installing a heatsink on the back of a PV module and integrating an internal heat sink in a PV module, the sheer amount of metal involved in producing a PV module with an integrated heat sink would be significantly less than installing a heatsink similar to COOLBACK. However, the cost of the thermal pads might be high as the Thermal Grizzly Minus 8 pads used in this project cost around 22.91€ per 10 cm x 10 cm square pad with a thickness of 0.5 mm (AZERTY, n.d.).

A simple analysis roughly estimates the material cost of manufacturing the final model, "Design 2".

Design 2 had:

- 6 strips of the thermal pad were used, having a thickness of 0.5 mm and an area of 10 cm x 2 cm. These thermal pads were used for the six cells on the sides of the module.

- 3 square pieces of thermal pad, having a thickness of 0.5 mm and an area of 5 cm x 5 cm used for the three cells in the middle of the modules.

- 12 strips of copper were used, having a thickness of 0.3 mm and an area of 10 cm x 5 cm. These copper strips were used for the six cells on the sides of the modules.

- 3 strips of copper, with a thickness of 0.3 mm and an area of 10 cm x 5 cm used for the three cells in the middle of the modules.

Each thermal pad is around 10 cmx10 cm, so for designing the 3x3 module, exactly two thermal pads are needed.

The density of copper is around 8.96 g/cm3 (Royal Society of Chemistry, 2022), so we would need around 201.6g of copper.

$$15strips * 10cm * 5cm * 0.03cm * \frac{8.96g}{cm^3} = 201.6g$$

The cost of copper is estimated to be around 7.12€/kg (Alibaba, 2022).

Hence the total estimated cost for the thermal pads is 2*22.91€= 45.82€, whereas the total estimated cost for the copper is 7.12€/kg*0.2016kg= 1.44 €.

Table 17- Cost breakdown for Design 2 module

	Total Material Cost in €	**Material Cost per cell in €/cell**
Thermal Pad	45.82	5.09
Copper	1.44	0.16

The additional cost of material per cell can be estimated to be around 5.25€/cell. Of course, this estimate solely depends on the cost of the newly added material. More costs are accrued due to the different manufacturing techniques needed to manufacture Design 2.

5 Conclusion

The performance of PV panels strongly depends on their temperature. An increase in the temperature of the cells leads to lower power output as the open-circuit voltage decreases. The increase in temperature also leads to a shorter lifetime for the module itself, as thermal cycling has a different effect on each material making up the solar module. Much research has been done to devise methods to decrease the temperature of the PV modules, reducing heat's effect on their electrical output.

This project aimed to study a potential passive cooling technique focusing on crystalline silicon (c-Si) based PV modules. It uses thermal pads and copper strips to form a thermal circuit behind the crystalline silicon cells to transfer the heat through an internal heatsink system toward the surrounding environment. The thermal pads could electrically insulate the copper strip from the IBC cells.

The initial concepts were tested on a single IBC cell. When the ideal concept was found, it was adjusted slightly and implemented on a 2x2 module. The most important design aspect was ensuring that the modified module's thermal resistivity was not higher than the original module. That was accomplished by having the thermal pad and copper strip indented by around 1.75 cm, which was close to the ideal calculated indentation length of 1.69 cm for a copper strip of thickness 0.3 mm. An offset of 4mm was needed to extract the copper strip from the back of the module. Some tests were performed to confirm the ideal concept for heat extraction on the 2 x 2 module, and the results showed that the calculated value was in agreement with the experimental data collected. Finally, a 3 x 3 module was manufactured with a new design to extract heat from the cell in the middle of the module. It was found that the temperature reduction potential of the internal heatsink concept was around 4.75°C.

During the experiment, it was found that the presence of copper makes the temperature of the PV cell more constant as the sudden increase or decrease in irradiance has a milder effect on the temperature of the PV cell. The heat suddenly added or removed due to the increase or decrease in irradiance will be compensated by the capacity of the copper strip to store heat.

Different environmental conditions lead to varying degrees of temperature reduction. An increase in the irradiance level causing a higher temperature in cells increases the temperature reduction achieved with the internal heatsink. Fluctuations in the level of irradiance in the case of clouds covering the sky, for example, lead to lower temperature reduction potential as the thickness of the copper strip combined with its high thermal capacity, lead to a delayed cooling effect when the sun disappears. The highest potential temperature reduction is expected during times of high irradiance levels throughout the day without disturbances mainly caused by clouds.

It was also observed that the temperature reduction achieved at each cell while comparing them to a Standard module was different. However, all cells saw a reduction in their temperature at different levels.

The material costs involved in integrating the internal heat sinks into the modules were calculated to be around 5.25€/cell. However, more research needs to be done to compare its cost with other passive module cooling techniques and to integrate the manufacturing costs.

Further research needs to be done on ways to accomplish the same amount of temperature reduction in all the cells of the module, to achieve an almost unified temperature profile. An idea to achieve a more unified temperature reduction from all the cells might be to use the extraction technique used for the middle cells in Design 2 by extracting the heat from the middle of the cells rather than at the edges.

A cost analysis comparing the cost of integrating internal heatsinks to the cost of other passive cooling techniques needs to be contemplated. A simpler design for the module's frame can also be implemented to reduce the amount of material needed in the updated frame and decrease the degree to which the backside area is covered.

Finally, it is also important to note that a significant challenge in developing these modified modules might be their production in large quantities. Research must be done to find a more straightforward method to manufacture these models. Creating the modules by hand requires extensive work and a transparent Tedlar to make sure the copper strips do not come into contact with the crystalline silicon cell.

Design Flow Chart

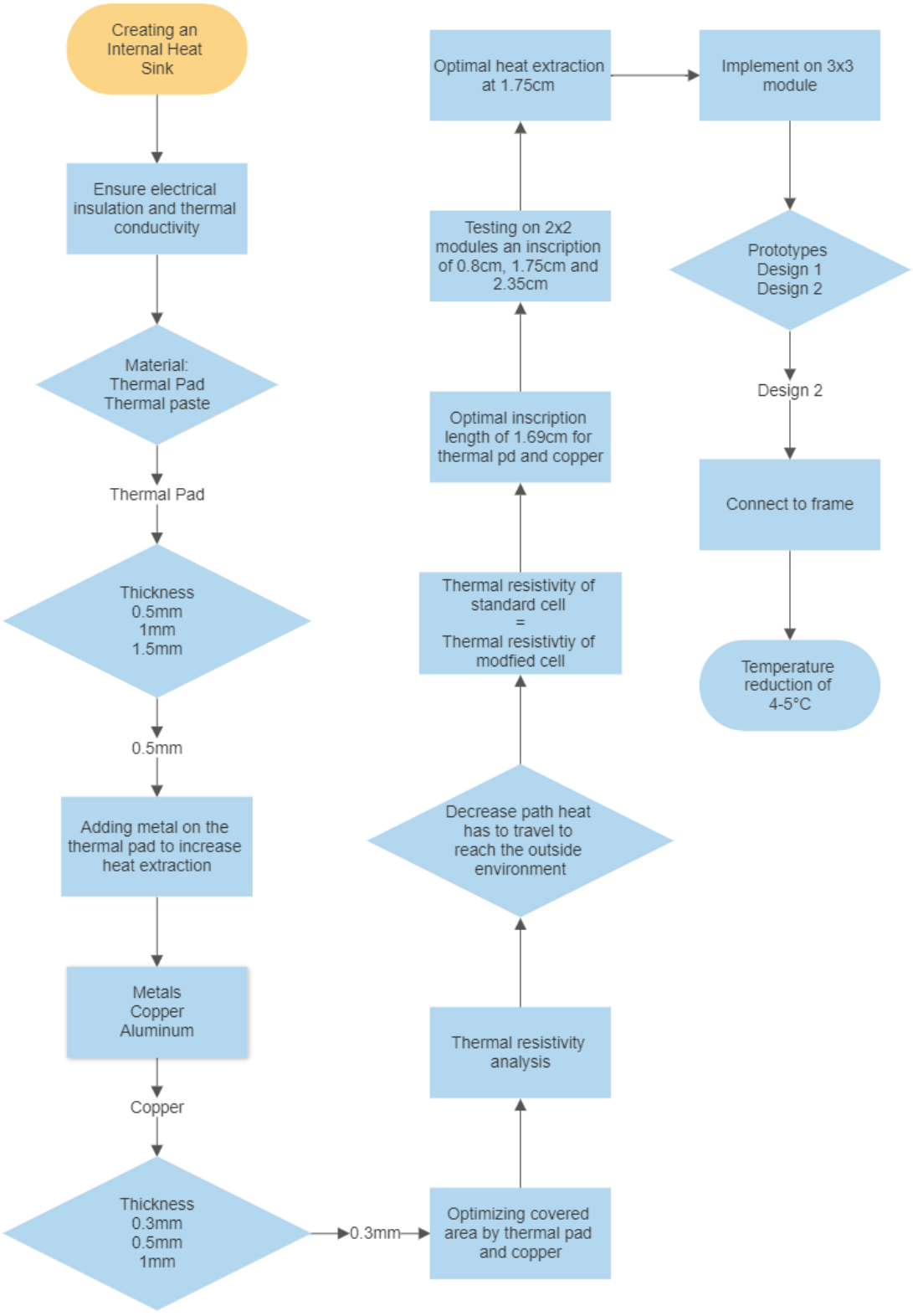

Appendix

Matlab code:

```
k_EVA=0.34;                 % Thermal conductivity of EVA

k_Tedlar=0.2;               % Thermal conductivity of EVA

k_Copper=356;               % Thermal conductivity of EVA

k_TP=8;                     % Thermal conductivity of EVA

t_Copper=0.3*10^-3;         % Thickness of Copper strip

t_EVA=0.4*10^-3;            % Thickness of EVA

t_Tedlar=0.5*10^-3;         % Thickness of Tedlar

t_TP=0.5*10^-3;             % Thickness of Thermal Pad

L_covered=10*10^-2;         % Length of the PV cell covered by heat pad and copper

X=0.001;                    % Length of indentation of heat pad and copper into the cell

S=0.4*10^-2;                % Length of the copper outside the cell and underneath the glass
layer

A_par=L_covered*X;          % Area of heat flow parallel to the PV cell covered by heat pad
and copper

A_per=t_Copper*10*10^-2;    % Area of heat flow parallel to the PV cell covered by heat
pad and copper

L=zeros(1000,1);            % Stores all values of the original thermal resistivity of the
covered part

M=zeros(1000,1);            % Stores all values of the new thermal resistivity of the covered
part

O=zeros(1000,1);            % Stores the increments of X

Area=0.015625;              % Area of the solar cell


R_original= (t_EVA)/(k_EVA*Area)+(t_Tedlar)/(k_Tedlar*Area);

% Calculates value of the original thermal resistivity of the covered part

R_new1=(t_EVA)/(k_EVA*(Area-A_par))+(t_Tedlar)/(k_Tedlar*(Area-A_par));
```

```
% Part of the cell which is not covered by thermal pad and copper

R_new2=     (t_TP)/(k_TP*A_par)+(t_Copper)/(k_Copper*A_par)+(X+S)/(k_Copper*A_per);
% Part of the cell which is covered by thermal pad and copper

R_new=R_new1*R_new2/(R_new1+R_new2);

% Calculation due to parallel heat flows

% Calculates value of the new thermal resistivity of the modified cell

for i=1:1000              % Iterates for different values of X

  A_par=10*10^-2*X;

  A_per=t_Copper*10*10^-2;

  R_original= (t_EVA)/(k_EVA*Area)+(t_Tedlar)/(k_Tedlar*Area);

  R_new1=(t_EVA)/(k_EVA*(Area-A_par))+(t_Tedlar)/(k_Tedlar*(Area-A_par));

  R_new2= (t_TP)/(k_TP*A_par)+(t_Copper)/(k_Copper*A_par)+(X+S)/(k_Copper*A_per);

  R_new=(R_new1*R_new2)/(R_new1+R_new2);

  L(i,1)=R_original;

  M(i,1)=R_new;

  O(i,1)=X;

  X=X+0.0001;

end

% Then the R_new matrix checked to find the value of R_new which is equal

% to R_original to identify how much copper can be inscribed into the cell

% without increasing the thermal resistivity of the cell
```

For a 0.3mm thickness copper strip, the optimal length of inscription was determined to be around 1.69cm.

References

(n.d.). Retrieved from AZERTY: https://azerty.nl/product/thermal-grizzly-minus-pad-8-thermische-mat/4041534

(2020). Retrieved from eternalsunspire: https://eternalsunspire.com/product/lass-aaa-large-area-steady-state/

(2021, August 27). Retrieved from Solar Magazine: https://solarmagazine.nl/nieuws-zonne-energie/i25152/fabrikant-achterwand-zonnepanelen-coolback-failliet-door-perfect-storm-doorstart-niet-uitgesloten

A.M. Elbreki, A. M. (2021). Experimental and economic analysis of passive cooling PV module. *Thermal Engineering 23*.

Ahmad El Mays, R. A. (2017). Improving Photovoltaic Panel Using Finned Plate of Aluminum. *ScienceDirect*.

Alibaba. (2022). Retrieved from https://www.alibaba.com/product-detail/Thickness-0-2mm-0-3mm-0_62331869268.html

Bayrak, F., Oztop, H. F., & Selimefendigil, F. (2019). *Effects of different fin parameters on temperature and efficiency for cooling of photovoltaic panels under natural convection.* Elsevier.

C.G. Popovici, S. H. (2016). Efficiency Improvement of Photovoltaic Panels by Using Air Cooled Heat Sinks. *Energy Procedia 85*, 425-432.

Chandrasekar, M., & Senthilkumar, T. (2015). *Experimental demonstration of enhanced solar energy utilization in flat PV (photovoltaic) modules cooled by heat spreaders in conjunction with cotton wick structures.* Elsevier.

Coolback. (2021, June 2). Retrieved from Dutch Dubai: https://dutchdubai.com/coolback/

Cuce, E., Bali, T., & Sekucoglu, S. A. (2011). *Effects of passive cooling on performance of silicon photovoltaic cells.* International Journal of Low-Carbon Technologies.

Escobar, B. L., Hernández, G. P., Ramírez, A. O., Blanco, L. R., Flores, L. L., Asencio, I. V., . . . Morales, E. R. (2021). *Analysis of Thermomechanical Stresses of a Photovoltaic Panel.* applied sciences.

Ethylene Vinyl Acetate (EVA). (2020, May 2020). Retrieved from MakeItFrom.com: https://www.makeitfrom.com/material-properties/Ethylene-Vinyl-Acetate-EVA

Grubišić-Čabo, F., Papadopoulos, A., Kragić, I., Čoko, D., & Nižetic, S. (2017). *Experimental investigation of the passive cooled free-standing photovoltaic panel with fixed aluminum fins on the backside surface.* Elsevier.

Indartono, Y. S., Suwono, A., & Pratama, F. Y. (2014). *Improving photovoltaics performance by using yellow petroleum jelly as phase change material.* Bandung.

J.G. Hernandez-Perez, J. C.-B.-L. (2021). Thermal performance of a discontinuous finned heatsink profile for PV. *Applied Thermal Engineering 184*.

Krauter, S. (2004). Increased electrical yield via water flow over the front of photovoltaic panels. *Solar Energy Materials and Solar Cells*, 131-137.

M.J. Huang, P. E. (2011). Natural convection in an internally finned phase change material heat sink. *Solar Energy Materials & Solar Cells*, 1598-1603.

Mazón-Hernández, R., García-Cascales, J. R., Vera-García, F., Káiser, A. S., & Zamora, B. (2013). *Improving the Electrical Parameters of a Photovoltaic Panel by Means of an Induced or Forced Air Stream.* International Journal of Photoenergy.

Miranda, A. (2022, Febraury 28). Retrieved from Solar ME: https://www.solarmeusa.com/blog/solarpanelstrength

novergy. (2020, July 29). Retrieved from https://www.novergysolar.com/understanding-the-degradation-phenomenon-in-solar-panels/

Nydia. (2017, June 21). *HAOMEI ALUMINUM*. Retrieved from https://www.aluminum-foil.net/the-aluminum-foil-uses/

Oh, J., Rammohan, B., Pavgi, A., Tatapudi, S., Tamizhmani, G., Kelly, G., & Bolen, M. (2018). *Reduction of PV Module Temperature.*

Photonics. (n.d.). Retrieved from https://www.photonics.com/Articles/Mirrors_Coating_Choice_Makes_a_Difference/a25501

Popovici, C. G., Hudişteanu, S. V., Mateescu, T. D., & Cherecheş, N.-C. (2016). *Efficiency Improvement of Photovoltaic Panels by Using Air Cooled Heat Sinks.*

R. Mazon-Hernandez, J. G.-C.-G. (10). Improving the electrical parameters of a photovoltaic panel by means of an induced or forced air stream. *Int. J. Photoenergy 2013*, Article ID 830968.

Royal Society of Chemistry. (2022). Retrieved from https://www.rsc.org/periodic-table/element/29/copper

S. Mehrotra S, P. R. (2014). Performance of a solar panel with water immersion cooling technique. *Int. J. Sci. Environ. Technol. 3*, 1161-1172.

S. Nizetic, D. C.-C. (2016). Water spray cooling technique applied on a photovoltaic panel: the performance response, Energy Convers. *Energy Convers. Manag. 108*, 287-296.

Selimefendigil, F., Bayrak, F., & Oztop, H. F. (2018). *Experimental analysis and dynamic modeling of a photovoltaic module with porous fins.* Elsevier.

Sharaf, M., Yousef, M., & Huzayyin, A. (2011). *Review of cooling techniques used to enhance the efciency.* Springer-Verlag.

Silva, P. S. (2017). *Infrared optical filters for passive cooling of c-Si solar modules.* TU Delft.

Teo, H., Lee, P., & Hawlader, M. (2012). *An active cooling system for photovoltaic modules.* Elsevier.

Weimar, N. D. (n.d.). *IBC Solar Cells*. Retrieved from sinocoltaics: https://sinovoltaics.com/learning-center/solar-cells/ibc-solar-cells/

Wongwuttanasatian, T., Sarikarin, T., & Suksri, A. (2020). *Performance enhancement of a photovoltaic module by passive cooling.* Elsevier.

Xinyue Han, Y. W. (2011). Electrical and thermal performance of silicon concentrator solar cells immersed in dielectric liquids. *Applied Energy*, 4481-4489.

Zhou, Z., Tkachenko, S., Bahl, P., Tavener, D., Silva, C. d., Timchenko, V., . . . Green, M. (2022). *Passive PV module cooling under free convection through vortex.* ELSEVIER.